



1     **Reframing gullies as recharge zones in dryland landscapes of the Loess Plateau, China**

2

3     Zhenxia Ji<sup>a,b,c,d</sup>, Alan D. Ziegler<sup>c</sup>, Li Wang<sup>a,b,c,d</sup>

4     <sup>a</sup> College of Natural Resources and Environment, Northwest A&F University, Yangling 712100, China

5     <sup>b</sup> College of Soil and Water Conservation Science and Engineering, Northwest A&F University, Yangling,  
6     712100, China

7     <sup>c</sup> State Key Laboratory of Soil and Water Conservation and Desertification Control, Northwest A&F  
8     University, Yangling 712100, China

9     <sup>d</sup> Institute of Soil and Water Conservation, Chinese Academy of Sciences and the Ministry of Water  
10    Resources, Yangling 712100, China

11    <sup>e</sup> Andaman Coastal Station for Research and Development, Kasetsart University, Ranong, Thailand

12

13    Correspondence to: Li Wang (wangli5208@nwsuaf.edu.cn)

14    State Key Laboratory of Soil and Water Conservation and Desertification Control, Institute of Soil and  
15    Water Conservation, Northwest A&F University.

16    Address: Xinong Road, #26, Yangling, Shaanxi Province 712100, China

17

18

19

20

21

22



## 23 Abstract

24 Large gullies in dryland landscapes are often viewed as indicators of land degradation, yet in some  
25 settings they may serve critical ecohydrological functions—supporting groundwater recharge and  
26 subsurface connectivity. In China’s Loess Plateau, we assess these functions in the Nianzhuang  
27 Catchment using a multi-indicator approach that integrates stable isotopes ( $\delta^2\text{H}$ ,  $\delta^{18}\text{O}$ ), chloride  
28 concentrations, and groundwater level fluctuations. Our results show that precipitation is the dominant  
29 source of recharge for shallow pore water within gully zones, while deeper fissure water is replenished  
30 more slowly through percolation from the upper layers. Restoration interventions—particularly check  
31 dams and ponds—act as focal points for groundwater infiltration, enhancing recharge in otherwise  
32 limited dryland systems. Estimated annual recharge (238–241 mm) accounts for over 43% of annual  
33 precipitation, far exceeding typical rates observed in nearby tableland and hilly areas. These findings  
34 revise prevailing assumptions by positioning gullies not simply as degraded features, but as  
35 hydrologically active zones that can buffer seasonal variability and support ecosystem resilience. The  
36 study advances a conceptual framework for using isotopic damping, chloride accumulation, and recharge  
37 partitioning as indicators of landscape function in semi-arid regions, offering valuable tools for dryland  
38 monitoring and restoration planning.

39  
40 **Keywords:** surface water, spring water, pore water, fissure water, connectivity

## 42 1. Introduction

43 Groundwater recharge is a critical yet poorly understood component of hydrological cycles in  
44 dryland catchments. It is shaped by the precipitation regime, surface landcover heterogeneity, the  
45 integrity of the subsurface regolith, the characteristics of the underlying bedrock, and human  
46 interventions (Vries and Simmers, 2002; Owuor et al., 2016; Salek et al., 2018; Xu and Beekman, 2019;  
47 Zhang et al., 2020; Li et al., 2024; Medici et al., 2024). Although favorable subsurface flow pathways can  
48 locally enhance recharge, dryland regions—situated along climatic ecotones and shaped by complex  
49 land–atmosphere–biosphere feedbacks—are highly sensitive to even modest shifts in water availability.  
50 Small changes in soil moisture or runoff routing can cascade across catchments at various scales,  
51 amplifying existing vulnerabilities to ecological and social systems (Nicholson, 2011; Huang et al., 2017;  
52 Berg et al., 2016). In these “fragile” and diverse landscapes, understanding the processes that govern



53 when, where, and how groundwater is replenished—including the countervailing influences of  
 54 vegetation dynamics, geomorphology, and engineered features—is essential for sustaining ecosystems,  
 55 securing water resources, and informing land restoration and catchment management (Gleeson et al.,  
 56 2016; Jasechko and Perrone, 2021; Scanlon et al., 2006).

57 Despite a growing body of research on groundwater recharge in (semi-)arid regions, significant  
 58 knowledge gaps remain in landscapes with pronounced spatial heterogeneity—such as slopes, hilltops,  
 59 and gullies—where infiltration pathways and recharge processes can diverge sharply over short distances  
 60 (Tooth, 2012; Manna et al., 2018; Letz et al., 2021). Among these landforms, gully systems—often  
 61 regarded as hallmarks of land degradation—may paradoxically serve as focal points for recharge,  
 62 capturing and infiltrating surface runoff during episodic rainfall events (Tan et al., 2017; Li et al., 2024;  
 63 Xue et al., 2025). Notably, gully systems may facilitate the rapid downslope transport of contaminants  
 64 such as agricultural contaminants and sediments (Lian et al., 2025; Qu et al., 2025). However, the role  
 65 of gullies in promoting vertical infiltration into groundwater is highly dependent on local subsurface  
 66 connectivity and permeability conditions. Moreover, their broader hydrological functions remain poorly  
 67 quantified—especially under the influence of widespread human interventions such as check dams and  
 68 artificial ponds. While these structures are typically designed to arrest land degradation, they can  
 69 substantially alter surface–subsurface connectivity and reshape recharge dynamics (Lamontagne et al.,  
 70 2021; Wang et al., 2023).

71 This study focuses on groundwater recharge in the gully systems in loess soils. Worldwide, loess  
 72 covers approximately 6% of the land surface area, forming discontinuous east–west belts in the mid-  
 73 latitude forest-steppe, steppe, and desert-steppe zones of both hemispheres (Liu, 1985; Pécsi, 1990; Li et  
 74 al., 2020). Among these, the Chinese Loess Plateau accounts for approximately 7.4% of the global loess  
 75 area (635,280 km<sup>2</sup>; Li et al., 2020). The setting for our investigation, semi-arid landscape has been shaped  
 76 by severe soil erosion, extensively modified by engineered landforms; and it is now characterized by  
 77 chronic water scarcity (Fu et al., 1999; Liu et al., 2017; Liu and Li, 2017; Li et al., 2021). In such  
 78 vulnerable environments, understanding the sources and sustainability of groundwater recharge is critical  
 79 for long-term water resource management (Ajjur and Baalousha, 2021; Meles et al., 2024). Groundwater  
 80 is a lifeline for rural communities in the hilly–gully region, yet scientific attention has largely bypassed  
 81 the gullies themselves. Most research has centered on recharge processes in tablelands and loess-covered  
 82 hills (Huang et al., 2011; Li et al., 2017; Lu, 2020; Wang et al., 2024), leaving the hydrological role of



83 gully systems—despite their striking prominence in the landscape—largely in the shadows (Liu et al.,  
 84 2011).

85 In this study, we integrate stable isotope analysis ( $\delta^2\text{H}$  and  $\delta^{18}\text{O}$ ), chloride concentration  
 86 measurements, water table fluctuation estimations, and hydro-statistical modeling to do the following: (i)  
 87 quantify pore water recharge rates; and (ii) trace flow paths among surface water, pore water, and fissure  
 88 water. This integrated approach aims to advance understanding of groundwater dynamics in complex  
 89 dryland terrains, generating process-based insights critical for sustainable water and land management  
 90 in gully-dominated systems—not only across the Loess Plateau, but in drylands globally.

91

## 92 **2. Hydro-geomorphological processes of the Loess Plateau**

93 The Loess Plateau in China stands out as one of the most ecologically and hydrologically distinctive  
 94 landscapes in the world (Fu et al., 2017). Spanning over 640,000 km<sup>2</sup>, it harbors the planet’s largest and  
 95 deepest loess deposits and has long served as a cradle of Chinese civilization (Li et al., 2021). The Loess  
 96 Plateau is also one of the most severely eroded regions in the world, shaped by the interplay of highly  
 97 erodible soils, intense summer storms, and a long history of farming on sloping lands (Shi and Shao,  
 98 2020). For centuries, steep hillslopes were cultivated without adequate soil conservation, removing  
 99 vegetation and exposing loess soils to heavy runoff during short, high-intensity monsoonal rains. These  
 100 conditions led to widespread gully formation—hallmarks of degradation tightly linked to land use and  
 101 rainfall extremes (Wang et al., 2006; Fu et al., 2011; Jin et al., 2020). The altered hydrological cycle on  
 102 the plateau has led to sharp declines in both streamflow and groundwater levels, resulting in acute water  
 103 scarcity across this arid to semi-arid region (200–750 mm annual rainfall) (Liang et al., 2015; Wang et  
 104 al., 2023; Chen et al., 2023). Understanding hydrological processes in this disturbed setting is essential  
 105 for guiding soil conservation, optimizing groundwater recharge, and ensuring the long-term  
 106 sustainability of water resources for both people and ecosystems.

107 The plateau’s complex stratigraphy—characterized by loess layers that can reach depths of up to  
 108 350 meters and average around 90 meters, with generally low permeability—governs groundwater  
 109 storage, recharge processes, and subsurface flow behavior (Qiao et al., 2017; Zhu et al., 2018). The region  
 110 is further divided into a range of distinctive landforms, or subregions, also shaped by variable erosion  
 111 processes (Yang et al., 2009): Loess Yuan (flat, high-elevation tablelands); Loess Liang (elongated  
 112 ridges); Loess Mao (rounded or oval-shaped hills); hills; and large-scale gullies (Fig. A1). While the



113 Loess Yuan remains relatively unincised by rivers/streams and maintains a smooth surface morphology,  
 114 the Liang and Mao formations exhibit profound dissection—shaped predominantly by fluvial erosion  
 115 and hillslope processes, respectively.

116 Hills in the region exhibit undulating terrain shaped by prolonged weathering and diffuse surface  
 117 runoff. In contrast, gully systems reflect both long-term geomorphic evolution and more recent  
 118 intensification driven by human activity—making them products of millennial-scale natural processes  
 119 and modern land-use pressures (Li et al., 2021; Jia et al., 2024). Prominent gully systems, which can  
 120 stretch for several kilometers, serve as primary conduits for concentrated runoff, facilitating the  
 121 downslope transfer of water, sediment, and eroded material. In doing so, they reflect and reinforce  
 122 ongoing landscape evolution and contribute to downstream sedimentation challenges (Zhu et al., 2018).

123 To combat degradation in the hilly–gully region, extensive afforestation efforts have been  
 124 implemented on hillslopes, while hydraulic structures—including check dams and ponds—have been  
 125 constructed in gullies (Feng et al., 2016; Xue et al., 2025). These interventions have significantly altered  
 126 runoff dynamics and water budgets (Huang et al., 2013; Yuan et al., 2022). While afforestation has  
 127 reduced soil moisture in hilly areas via enhanced evapotranspiration (~8.7%), hydraulic engineering has  
 128 increased soil moisture in gullies by 21% (Wang et al., 2019, 2020; Zhao et al., 2019, 2024). Notably,  
 129 the additional water retained within gully systems offsets an estimated 44% of the water loss from  
 130 afforested hillslopes, partially reshaping the local water cycle (He et al., 2020; Zhao et al., 2024). Under  
 131 such intensive human modification, the Plateau’s inherently complex landforms and stratigraphy have  
 132 come to exert even greater control over groundwater recharge dynamics (Li et al., 2024).

133 Research on groundwater recharge in the Loess Plateau’s gully regions is incomplete, with most  
 134 studies concentrating on deep profiles in tableland and hilly areas (Huang et al., 2011; Li et al., 2017; Lu,  
 135 2021; Wang et al., 2024). Early scholars proposed that fissures and caves in loess enabled preferential  
 136 flow, allowing precipitation to reach groundwater (Yan and Wang, 1983). However, Xu et al. (1993)  
 137 argued that the vertical fractures in the loess layer do not facilitate continuous water movement; instead,  
 138 the vertical joints and large pores may act as barriers, which is caused by air-blocking effects. Li (2001)  
 139 argued that the formation of dried soil layers further disrupts groundwater recharge pathways, causing  
 140 precipitation to cycle within the soil–plant–atmosphere system rather than contributing meaningfully to  
 141 groundwater recharge. In recent years, researchers have applied isotope tracing, hydrochemical analysis,  
 142 and model simulations to study recharge mechanisms in deep-loess regions (Lu, 2020; Xiang, 2020; Shi



et al., 2021; Wang et al., 2023). These studies suggest that recharge occurs primarily through slow piston flow, with precipitation infiltrating thick soil profiles, slowly recharging groundwater in a process that can take decades to hundreds of years (Huang et al., 2013; Tan et al., 2017; Li et al., 2024). Piston flow refers to a type of water movement through the unsaturated (vadose) zone or an aquifer where newly infiltrating water pushes the existing water downward, much like a piston in a cylinder (Gee and Hillel, 1988).

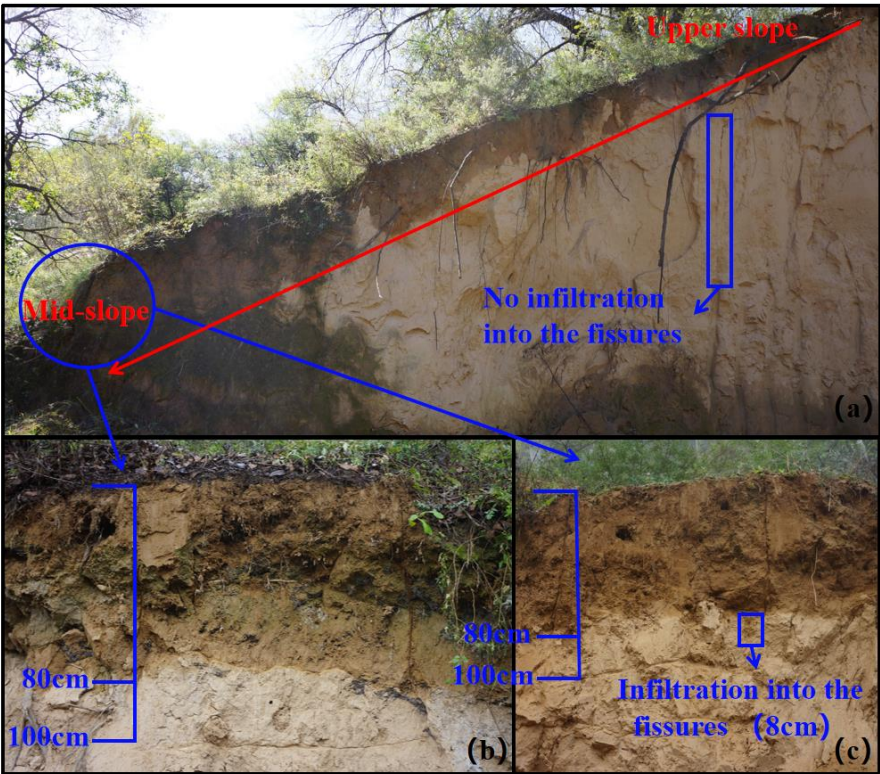
However, deep-profile recharge mechanisms observed in tableland and hilly areas may not apply to gully landscapes on the plateau. Regional-scale analyses of 40 years of soil moisture data show that precipitation infiltration in thick loess deposits is typically restricted to shallow depths, even though loess thickness in tableland and hilly areas ranges from 56.5 to 204.5 m (Wang et al., 2024; Qiao et al., 2017). In contrast, loess in gully regions is generally much thinner—often less than 50 m (Zhu et al., 2018). Infiltration on loess slopes appears similarly limited (Fig. 1).

During field observations in the 2023 rainy season in the Nianzhuang Catchment, located in the hilly–gully region of the Loess Plateau, we found little evidence of preferential flow through cracks or macropores. Instead, infiltration appeared slow and driven predominantly percolation through the matrix (Wang et al., 2024). That year, total rainfall from May to October amounted to 420 mm, with 115 mm falling in September alone. Consistent with earlier studies (Xu et al., 1993; Li, 2001), only a few surface cracks showed signs of infiltration, and even then, the water was absorbed by surrounding soils and failed to infiltrate deeper (Fig. 1c). Moreover, soil profiles remained unsaturated from the surface to deeper layers, indicating that precipitation infiltration is generally insufficient to recharge groundwater (Qiao et al., 2017). After a 41-mm rainfall event occurring over four days, infiltration depths reached only 20–30 cm at the top of the slope, compared with 80 cm at mid-slope positions (Fig. 1b, c).

These patterns indicate that infiltration is limited at higher slope elevations, with much of the water moving laterally downslope as overland flow and accumulating in gully areas, where conditions are more conducive to groundwater recharge. Previous studies have shown that gullies and other topographic depressions function as key recharge zones, enabling concentrated surface flows to infiltrate more deeply and contribute to subsurface water stores (Gates et al., 2011; Liu et al., 2011; Zhao et al., 2021). Building on this foundation, advancing our understanding of gully-driven recharge requires targeted investigation of interactions among precipitation, surface water, and groundwater—particularly the flow paths and magnitudes of near-surface infiltration. These insights are critical for guiding water resource



173 management and ecological restoration across the Loess Plateau.



174  
175 Fig. 1. The topographic profile of the Nianzhuang catchment in the hilly region of the Loess Plateau. Full  
176 profile from the top to mid-slope (a); two repeated mid-slope profiles (b, c). The photo was taken after a  
177 41 mm rainfall event over four days. Subsequent measurements showed that infiltration depths reached  
178 only 20–30 cm at the top of the slope, compared to approximately 80 cm at the mid-slope positions.

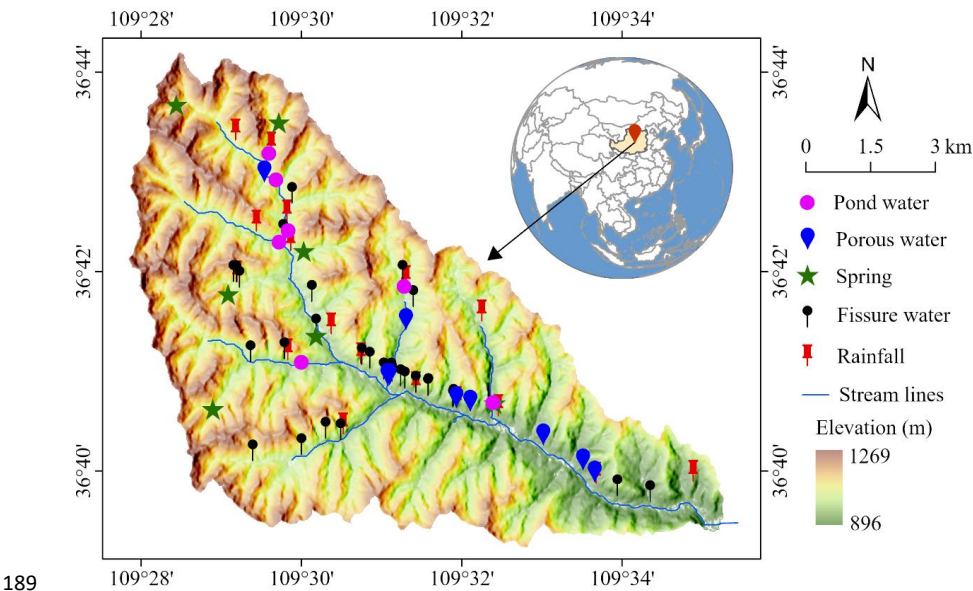
179  
180 **3. Sampling site**

181 The Nianzhuang Catchment is located northwest of Yan'an City in Shaanxi Province, China  
182 (approximately 36°42'N, 109°31'E). As a tributary of the Yanhe River—which ultimately flows into the  
183 Yellow River—the catchment spans 53.94 km<sup>2</sup> and includes the well-studied Yangjuangou sub-  
184 catchment (3.11 km<sup>2</sup>; ~36°35'N, 109°32'E), previously investigated in numerous hydrological and  
185 ecological studies (Fu et al., 1999; Liu and Li, 2017). Elevation ranges from 896 to 1,269 m, with terrain  
186 gradually sloping from northwest to southeast (Fig. 2). The region experiences a semi-arid continental  
187 monsoon climate, with a mean annual precipitation of approximately 550 ± 100 mm, concentrated





188 between July and September (Liu et al., 2017).



190 Fig. 2. The geographical location and sampling sites for rainfall, pond water, pore water, spring water,  
191 and fissure water in the Nianzhuang catchment. The Nianzhuang catchment is located in the hilly and  
192 gully region of the central Loess Plateau, with elevations ranging from 869 to 1269 m. The average depth  
193 of pore water wells is  $8.0 \pm 1.5$  m (range: 4–10 m), while that of fissure water wells is  $57.6 \pm 29.2$  m  
194 (range: 25–170 m). These sampling sites represent locations where both rainy and dry season samples  
195 were collected, and are all situated within the gully areas of the catchment.

196 The catchment features highly dissected loess terrain, with characteristic soils and landforms such  
197 as Loess Liang (ridges), Loess Mao (mounds), and steep loess slopes (Cai et al., 2019). Gullies—often  
198 “V”- or “U”-shaped—dominate the lower-lying regions and serve as important recharge zones. These  
199 landforms, together with ancient landslides, minor collapses, and sinkholes, highlight the geomorphic  
200 instability of the Loess Plateau landscape (Li et al., 2021).

201 The stratigraphy of the catchment reflects the typical layered structure of the Loess Plateau, which  
202 plays a key role in controlling groundwater recharge. In upland hilly areas, thick loess deposits overlie  
203 bedrock, with the Upper Pleistocene Malan Loess—light grayish-yellow, loosely textured, and silt-rich  
204 (>60%)—characterized by well-developed vertical joints and abundant hematite and goethite. Beneath  
205 it lies the Middle Pleistocene Lishi Loess, a grayish-yellow to light brown unit with prominent jointing  
206 and higher iron mineral content. Below the loess, the Neogene Red Clay appears as a distinctly reddish,

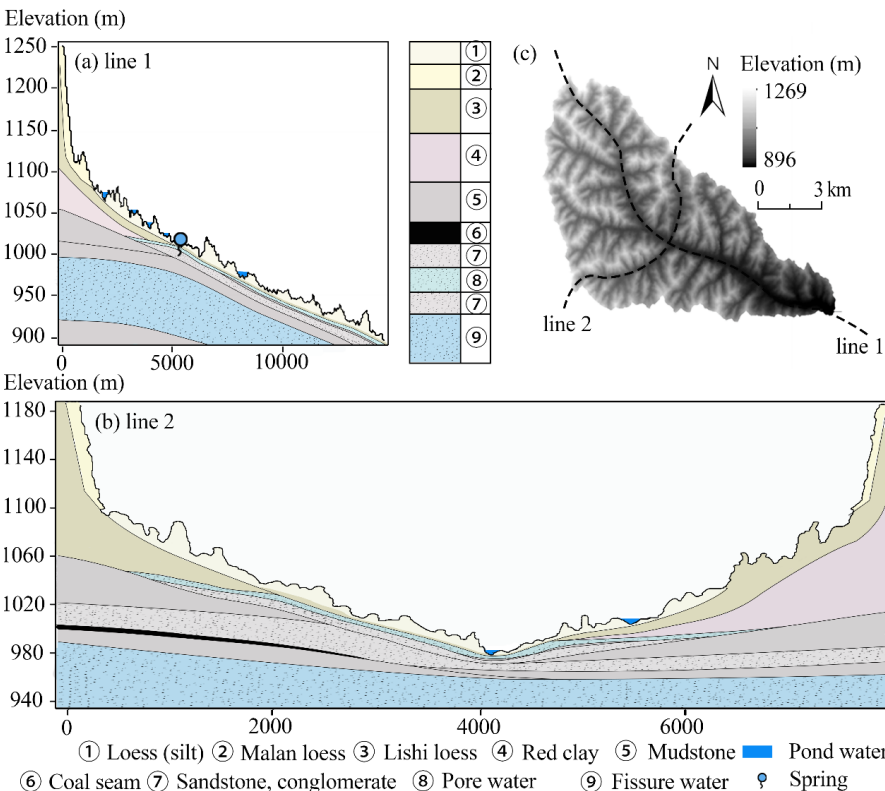




207 calcareous nodule-bearing aquitard due to its low permeability. The entire sequence rests on Jurassic  
208 sandstone–conglomerate bedrock, composed mainly of quartz-rich fluvial–lacustrine deposits.

209 Loess thickness in the Liang and Mao regions often exceeds 150 meters, resulting in deep water  
210 tables and limited groundwater accessibility. In contrast, gully zones exhibit distinctly different  
211 hydrogeological characteristics. Here, thinner loess layers overlie Neogene and Jurassic formations,  
212 sometimes interbedded with coal seams up to 5 meters thick (Fig. 3a–c). The significant reduction in  
213 loess thickness—combined with the relatively high permeability of Neogene coarse sandstone and  
214 conglomerate (7.5–36.19 m/d)—creates favorable conditions for infiltration and focused recharge.

215 These dynamics are especially evident at gully heads, where surface runoff from adjacent uplands  
216 converges and infiltrates, forming efficient recharge zones. As a result, gully areas tend to have shallower  
217 water tables and more rapid water renewal, making them more suitable for domestic groundwater use.  
218 Springs frequently emerge at gully bottoms where lateral flow is facilitated at the loess–bedrock interface.  
219 Streams in this dry environment are largely intermittent.



220  
221 Fig. 3. Hydrogeologic cross-section of the study area. Cross-section along Line 1 (Northwest-Southeast)



(a); cross-section along Line 2 (Southwest-Northeast) (b); location map of Line 1 and Line 2 within the study area (c). The Malan Loess (11.7–12.6 Ka BP) and Lishi Loess (12.6–78.1Ka BP) are two major Quaternary loess stratigraphic units in China. Based on hydrogeological research, the stratigraphy of the hilly region features a multi-layer structure from top to bottom: Upper Pleistocene Malan Loess, Middle Pleistocene Lishi Loess, Neogene Red Clay and Mudstone (2.58–23.03 Ma BP), and Jurassic Sandstone and Conglomerate (145–201.3 Ma BP). In the gully region, the stratigraphy includes Holocene loess (silt, 11.7 ka BP–present), Middle Pleistocene Lishi Loess, Neogene sandstone and mudstone, and Jurassic sandstone and conglomerate, with some areas containing coal seams up to 5 meters thick.

Groundwater in the catchment can be broadly categorized into three types: pore water, spring water, and fissure water. Pore water is stored in permeable sandstone and conglomerate aquifers beneath loess and above mudstone or red clay. Conceptually, “pore water” here refers to groundwater in a saturated aquifer, not to soil moisture. Fissure water occurs within fractured bedrock aquifers but is spatially discontinuous due to irregular fissure development. Hydraulic conductivity in these sandstone and conglomerate aquifers ranges from 0.0218 to 0.471 m/day (Cai et al., 2019). Spring water emerges primarily at gully bases—especially in upper catchments—and originates from both pore and fissure sources, possibly supplemented by surface or pond water.

Over recent decades, landscape rehabilitation through the Grain for Green Project and land reshaping under the Gully Land Consolidation Project have significantly altered the hydrological regime (Fu et al., 1999; Liu et al., 2017). Historically, surface runoff in the degraded catchment was flashy and episodic due to sparse vegetation. However, ecological restoration and small-scale engineering interventions—such as check dams, terraces, roads, and ponds—have moderated surface hydrology. Surface runoff, generated primarily during storm events, now contributes alongside delayed baseflow from groundwater recharge and interflow. The latter is often limited by the thick unsaturated zone in upland loess areas but may be enhanced in gully regions, where stratigraphy and land use favor infiltration (Wang et al., 2024; Gates et al., 2011). Gully areas also contain numerous check dams and ponds, with most water sourced from Hortonian overland flow and direct rainfall. These small water bodies, often constructed for erosion control and water retention, influence local hydrological dynamics and may play a role in enhancing infiltration and recharge.

250

#### 251 4. Methods



Our approach integrates stable isotope analysis ( $\delta^2\text{H}$  and  $\delta^{18}\text{O}$ ), chloride concentration analysis, and water table fluctuation monitoring to investigate groundwater recharge dynamics. The isotopic composition of water bodies reflects both their origins and the processes they undergo—such as evaporation, infiltration, and mixing (Wan and Liu, 2016; Kumar et al., 2019; Dasgupta et al., 2024). Precipitation, surface water, and groundwater typically exhibit distinct isotopic signatures due to these differing pathways (Gleeson et al., 2016; Kuang et al., 2019; Al-Oqaili et al., 2020). When isotopic patterns among water sources converge, it often indicates strong hydrological connectivity (Yang and Wang, 2023). Because stable isotopes behave conservatively, they serve as effective tracers of water sources and flow paths (Gleeson et al., 2016; Al-Oqaili et al., 2020; Dasgupta et al., 2024). In parallel, water table fluctuation (WTF) monitoring provides a means of estimating recharge by observing changes in groundwater levels in response to precipitation events (Nachabe, 2002; Heppner and Nimmo, 2005; Gumula-Kawęcka et al., 2022). By combining these complementary methods, this study aims to elucidate groundwater recharge pathways and quantify recharge rates in gully regions—thereby identifying key recharge zones and advancing our understanding of groundwater processes in the Loess Plateau.

#### 4.1. Field measurements of hydrological data

Precipitation was collected from October 24, 2023, to October 24, 2024, using a weather station situated in an open field within the catchment. Continuous groundwater level data were recorded from September 24, 2023, to December 20, 2024. Groundwater pressure and temperature were monitored using Onset HOBO U20-001-03 sensors (20 m range), and water table levels were calculated based on the measured pressure data. The conversion relationship between water pressure and groundwater level is given by  $Y = 0.86 \times X - 22.1$  where  $Y$  represents the groundwater level and  $X$  represents the water pressure. Notably, the monitoring well is located in the pore water layer of the gully region. The well is hand-dug (1.1 m wide, 10 m deep) and is unaffected by human activities.

Soil physical properties were assessed using the cutting ring method, based on undisturbed soil cores collected at five depth intervals: 0–10, 10–20, 20–30, 30–40, and 40–50 cm. Quadruplicate samples were taken near groundwater monitoring wells in the gully using pre-weighed cutting cylinders. The samples were immediately transported to the laboratory for analysis. Bulk density, capillary porosity, non-capillary porosity, total porosity, and field water capacity were determined following the LY/T 1215-1999 standard for forest soil water-physical properties. Soil particle size distribution was analyzed using



a laser particle size analyzer at the College of Natural Resources and Environment, Northwest A&F University. Soil texture classification followed the USDA system: sand (0.05–2 mm), silt (0.002–0.05 mm), and clay (<0.002 mm) (Dane et al., 2002).

285

## 286 4.2 Water sampling

A total of 181 water samples were collected from various locations in rainy season (September 2023, 99 samples) and dry season (April 2024, 82 samples); see Fig. 2. Rainy season samples included 48 from rainfall, 7 from pond water (water retention reservoirs), 9 from spring water, 9 from pore water, and 26 from fissure water. During the dry season, samples included 31 from rainfall, 6 from pond water, 8 from pore water, 29 from fissure water, and 8 from spring water.

Pore water was collected from several shallow, hand-dug wells measuring approximately 1.1 meters in diameter and 4–10 meters in depth. Fissure water was sampled from deeper, narrow-diameter wells (0.2 meters wide, 25–170 meters deep). In areas with numerous deep wells, we employed random sampling to ensure representative coverage of fissure water sources. To minimize the risk of collecting stagnant water, all pore and fissure water wells were purged for 10–15 minutes prior to sampling. Spring water was collected directly from natural discharge points, although most springs in the region exhibit low flow rates—typically less than 0.1 L/s, occasionally reaching up to 0.2 L/s.

A total of 18 bulk rainfall collectors were randomly and evenly distributed across the 54 km<sup>2</sup> study area, and samples were collected immediately following rainfall events. For nighttime precipitation, samples were collected the next morning at 6:00 AM. During the study period, we collected two types of precipitation samples: (1) spatial samples from individual events (18 in the rainy season and 15 in the dry season) across the catchment, capturing spatial variability; and (2) sequential events at a fixed station (30 in the rainy season and 16 in the dry season), characterizing seasonal inputs.

During sampling, 100 mL collection bottles were rinsed two to three times with the sample water, then slowly filled to minimize air exposure. After filling, the bottles were tightly sealed with screw caps and further secured with Parafilm to prevent evaporation and contamination. All samples were immediately stored in a portable cooler at 4°C and transported to the laboratory for isotopic and chloride concentration analysis.

310

## 311 4.3. Isotopic analysis



The  $\delta^2\text{H}$  and  $\delta^{18}\text{O}$  values of the water samples were determined using a Los Gatos Research liquid water isotope analyzer (Model 912-0032, LGR Inc., California, USA) at the Institute of Water-Saving Agriculture in Arid Areas of China, Northwest A&F University. Each sample was injected six times in the following sequence: three standard injections, followed by six natural sample injections, and then three additional standard injections. The isotope ratios were calculated using the average composition from injections 4 through 6.

Isotope values are expressed in delta ( $\delta$ ) notation, which represents the relative difference in isotope ratio between a sample and the Vienna Standard Mean Ocean Water (VSMOW) reference. The measurement precision was  $\pm 0.5\text{‰}$  for  $\delta^2\text{H}$  and  $\pm 0.1\text{‰}$  for  $\delta^{18}\text{O}$ . The delta values were calculated using the following equations:

$$\delta^{18}\text{O} = \left( \frac{R_{\text{sample}}}{R_{\text{standard}}} \right) - 1 \quad (1)$$

$$\delta^2\text{H} = \left( \frac{R_{\text{sample}}}{R_{\text{standard}}} \right) - 1 \quad (2)$$

where  $R_{\text{sample}}$  and  $R_{\text{standard}}$  are the ratios of heavy to light isotopes ( $^{18}\text{O}/^{16}\text{O}$  or  $^2\text{H}/^1\text{H}$ ) in the sample and the standard, respectively. Results are expressed in per mil (‰).

326

#### 327 4.4. Mixing process of different water bodies

Inverse transit time proxies (ITTPs) were calculated to assess differences in water transit times and mixing processes across various water bodies (Tetzlaff et al., 2009). ITTPs are defined as the ratio of the standard deviation of  $\delta^{18}\text{O}$  in the water sample (e.g., pond water, spring water, pore water, or fissure water) to that in precipitation over the same time period:

$$\text{ITTP} = \frac{\sigma_{\delta^{18}\text{O}}(\text{sample})}{\sigma_{\delta^{18}\text{O}}(\text{precipitation})} \quad (3)$$

This ratio captures the attenuation of seasonal isotopic variability in  $\delta^{18}\text{O}$  as water moves through the landscape. In general, ITTP values less than 1 indicate substantial damping of the precipitation signal—consistent with longer water residence times, greater mixing, and larger storage volumes. Conversely, values approaching 1 suggest minimal damping and rapid flow paths.

However, interpretation of ITTPs must also account for fractionation processes. In particular, evapotranspiration (ET) selectively removes lighter isotopes ( $^{16}\text{O}$ ), enriching the remaining water in heavier isotopes ( $^{18}\text{O}$ ). This enrichment can artificially increase the variance of  $\delta^{18}\text{O}$  in near-surface or shallow soil water compartments, inflating ITTP values even in systems with relatively slow transit times



(Tetzlaff et al., 2009). This is especially relevant in arid and semi-arid regions, where ET can dominate the water balance during dry seasons.

343

#### 344 **4.5. Hydraulic connectivity estimation**

345 Structural Equation Modeling (SEM) has been widely applied in water science to evaluate complex  
 346 causal relationships among hydrological, geological, and anthropogenic variables—particularly in  
 347 studies of groundwater contamination and water quality degradation (Wu, 2010; Lupi et al., 2019; Xie et  
 348 al., 2025). In this study, we adapted SEM as an exploratory framework to assess hypothesized recharge  
 349 linkages among water sources, using dual-isotope ( $\delta^2\text{H}$ – $\delta^{18}\text{O}$ ) data from rainfall, pond water, spring water,  
 350 pore water, and fissure water. Although SEM is not a mass-conserving approach and is less commonly  
 351 used in isotope-based flowpath analysis, it enables estimation of statistically significant relationships and  
 352 indirect linkages within a hypothesized recharge system.

353 Given the potential for isotopic signatures to be altered by evaporation, mixing, or other non-  
 354 conservative processes, results must be interpreted with caution. Pathways with p-values > 0.05 were  
 355 excluded during model refinement, and the final model met standard goodness-of-fit criteria (degrees of  
 356 freedom < 3, RMSEA < 0.05, CFI > 0.95, NFI > 0.95). SEM analysis was conducted using SPSS Amos  
 357 26.0 (IBM SPSS, Chicago, Illinois, USA).

358 In addition, we applied variance partitioning to evaluate the relative contributions of different water  
 359 sources to pore and fissure water. This method decomposes the total variance in isotopic composition  
 360 into components attributable to individual sources (e.g., precipitation, pond water, spring water), offering  
 361 a complementary estimate of source influence. While useful, this approach remains subject to the same  
 362 limitations as SEM—particularly the challenges of isotopic overlap and limited resolution in  
 363 environments affected by mixing and evaporation (Lai et al., 2022).

364 To further constrain recharge pathways, we incorporated chloride ion ( $\text{Cl}^-$ ) as a conservative tracer.  
 365 Unlike stable isotopes, chloride is unaffected by evaporation or biological processes, making it a robust  
 366 indicator for identifying recharge sources and tracking subsurface water movement. Chloride  
 367 concentrations in all water samples were analyzed using an ion chromatograph (DIONEX ICS-1100) at  
 368 the College of Natural Resources and Environment, Northwest A&F University, China. Each sample was  
 369 analyzed in triplicate, with charge balance errors maintained below 5% to ensure analytical accuracy.  
 370 This rigorous approach enhances the reliability of chloride data, supporting its integration with isotopic



371 indicators in source attribution.

372

#### 373 4.6. Groundwater recharge

374 Groundwater recharge in the gully zone is quantified using the water table fluctuation (WTF)  
 375 method, which infers recharge and discharge events from temporal changes in groundwater levels (Healy  
 376 and Cook, 2002; Gumuła-Kawęcka et al., 2022). We recognize that recharge can originate from three  
 377 hydrological sources: (1) surface water; (2) the unsaturated zone (3) and the saturated zone (Scanlon et  
 378 al., 2022; Wang et al., 2024). Among these, estimates based on the saturated zone are generally most  
 379 reliable, as recharge from the unsaturated zone reflects potential inputs that may never reach the water  
 380 table (Beven and Germann, 2013; Huang et al., 2019). The WTF method is widely used for estimating  
 381 saturated zone recharge due to its high temporal resolution and conceptual simplicity (Xu et al., 2024).  
 382 Based on previous site-specific studies (Wang et al., 2024), this method is well-suited for our analysis.

383 The water table fluctuation method assumes that changes in the groundwater table result solely from  
 384 recharge or discharge, assuming a constant specific yield ( $S_y$ ) over time (Healy and Cook, 2002; Obuobie  
 385 et al., 2012). The formula is as follows:

$$386 \quad R_i = S_y \frac{\Delta H_i}{\Delta t} \quad (4)$$

387 where,  $R$  is the groundwater recharge (mm),  $S_y$  is the specific yield of the aquifer,  $\Delta H_i$  (where  
 388  $\Delta H_i > 0$ ) is the groundwater table rise caused by recharge between day  $i - 1$  and  $i$ , and  $t$  is time period.  
 389 Specific yield, which represents the proportion of water that drains freely from the saturated zone under  
 390 gravity, was determined using two methods: the soil texture empirical method and the test pit method  
 391 (Liang, 2016).

392 Empirical values for soil texture are referenced in Table A1. The test pit method for estimating  $S_y$  is  
 393 described as follows:

$$394 \quad S_y = TP - FWC \quad (5)$$

395 where,  $TP$  (total porosity) and  $FWC$  (field water capacity) were measured using the cutting ring  
 396 method.

397 We applied two methods to calculate the daily groundwater table increments ( $\Delta H_i$ ). The RISE  
 398 method assumes that recharge occurs only when the groundwater table elevation increases between two  
 399 consecutive days (Gumuła-Kawęcka et al., 2022). Thus,  $\Delta H_i = H_i - H_{i-1}$  if  $H_i > H_{i-1}$ , otherwise,





400  $\Delta H_i = 0$ . The master recession curve (MRC) method assumes that, in the absence of recharge, the  
 401 groundwater table declines daily by a specific amount ( $\Delta H_{MRCi}$ ). This amount represents a simplified  
 402 approximation of discharge processes in the aquifer, particularly lateral outflow to nearby surface water  
 403 bodies. MRC establishes a functional relationship between a daily decrement of the water table ( $\Delta H_{MRCi}$ )  
 404 and the water table elevation ( $H_{i-1}$ ) during periods without recharge.

$$405 \quad \Delta H_{MRCi} = A \cdot H_{i-1} + B \quad (6)$$

406 where, the coefficients A and B were fitted for each piezometer based on data from periods of  
 407 continuous groundwater table decreases lasting longer than two weeks. The daily water table increment  
 408 due to recharge was then calculated as:  $\Delta H_i = H_i - H_{i-1} + \Delta H_{MRCi}$  if  $H_i > (H_{i-1} - \Delta H_{MRCi})$ ,  
 409 otherwise,  $\Delta H = 0$ .

410 Notably, we used water dynamics from October 24, 2023, to October 24, 2024, to calculate pore  
 411 water recharge, as this period exhibited clear groundwater fluctuations, making it more representative.

412

## 413 **5. Results**

### 414 **5.1. Soil properties**

415 The upper 50 cm of the soil profile is composed primarily of silt ( $64.6 \pm 0.6\%$ ), with smaller but  
 416 nearly equal proportions of clay ( $18.0 \pm 1.3\%$ ) and sand ( $17.4 \pm 1.6\%$ ), classifying the loess as silt loam  
 417 according to the International Union of Soil Sciences (IUSS) scheme (Fig. 4a). Total porosity and field  
 418 water capacity decreased slightly with depth, averaging  $24.5 \pm 1.9\%$  and  $21.3 \pm 1.7\%$ , respectively (Fig.  
 419 4b). Specific yield remained relatively consistent within the 10–50 cm depth interval, averaging  
 420  $3.2 \pm 0.8\%$ —falling within the expected empirical range for silt loam soils (2%–7%) (Fig. 4c).

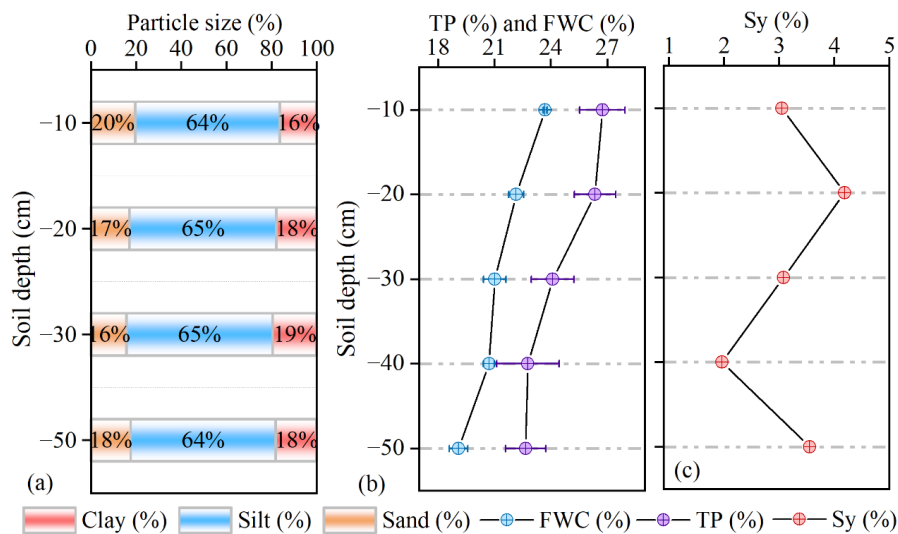


Fig. 4. Vertical variation in soil texture and water retention characteristics in the gully region of the Loess Plateau. (a) Soil particle size distribution by depth, showing relatively uniform composition across layers (10–50 cm), dominated by silt (64–65%), with moderate clay (16–20%) and low sand (16–20%) content. This fine-textured profile supports high moisture retention and slows infiltration, promoting delayed recharge. (b) Depth profiles of total porosity (TP) and field water capacity (FWC) reveal increases with depth to 40 cm, with FWC reaching ~27%, suggesting greater water-holding capacity in subsoil layers and enhanced buffering of infiltrated water. (c) Specific yield (Sy) peaks at -20 cm (4.5%) but decreases with depth, indicating shallower layers are more responsive to infiltration and release, while deeper layers tend to store water with minimal drainage. Collectively, these physical properties reflect a vertically stratified soil system where near-surface layers regulate infiltration pulses, and deeper layers act as long-term storage, shaping the timing and magnitude of subsurface recharge.

## 5.2. Hydrological signatures of rainfall, surface water, and groundwater sources

Pond water and rainfall exhibit similar spatial isotopic patterns, with more positive  $\delta^2\text{H}$  values ( $\delta^2\text{H} > -55\text{‰}$ ) than spring water, pore water, and fissure water (Fig. 5a, b). These values are line with the notion of direct rainfall and Hortonian runoff are the primary source of pond water. In contrast, the  $\delta^2\text{H}$  values of pore, spring, and fissure water show little seasonal variation and are consistently more negative ( $\delta^2\text{H} < -55\text{‰}$ ), than mean rainfall, indicating longer residence times and reduced evaporative influence.

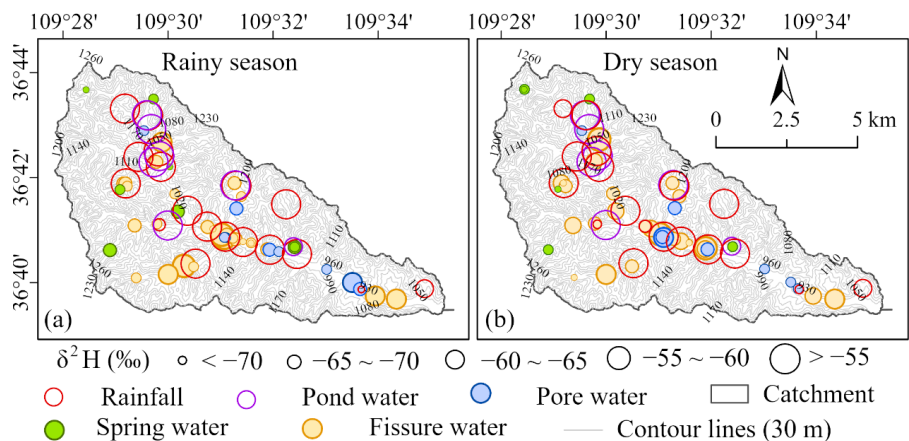


Fig. 5. The spatial distributions of  $\delta^2\text{H}$  values during the (a) rainy season and (b) dry season for rainfall, pond water, spring, pore water, and fissure water in the gully region of the Loess Plateau. To highlight spatial differences among water sources,  $\delta^2\text{H}$  values were classified into five intervals:  $< -70\text{‰}$ ,  $-70$  to  $-65\text{‰}$ ,  $-65$  to  $-60\text{‰}$ ,  $-60$  to  $-55\text{‰}$ , and  $> -55\text{‰}$ . Sampling points are color-coded by water type: red for rainfall, purple for pond water, blue for pore water, green for spring water, and orange for fissure water.

The  $\delta^2\text{H}$ – $\delta^{18}\text{O}$  relationships and box plots for each water source reveal key insights into the dominant hydrological processes occurring during the rainy season (Fig. 6). Firstly, rainfall follows a Local Meteoric Water Line (LMWL) of  $\delta^2\text{H} = 7.7 \cdot \delta^{18}\text{O} + 8.9$  ( $R^2 = 0.95$ ), which is closely aligned—though slightly offset—from the Global Meteoric Water Line (GMWL:  $\delta^2\text{H} = 8 \cdot \delta^{18}\text{O} + 10$ ) (rainy season; Fig. 6a, c). This alignment confirms that precipitation in the region has a typical meteoric origin. Additionally, minimal evaporative enrichment occurred prior to collection. The relatively wide interquartile range of rainfall  $\delta^{18}\text{O}$  values suggests that precipitation was derived from storm systems with considerable isotopic variability, reflecting differences in rainfall intensity, air mass origin, and temperature (Kumar et al., 2019; Oqaili et al., 2020; Dasgupta et al., 2024). However, this variability remains moderate compared with global patterns that span extreme rainfall events and broader climatic gradients.

Pond water, in contrast, exhibits a clear evaporation signature with a shallower slope of  $\delta^2\text{H} = 5.6 \cdot \delta^{18}\text{O} - 17.1$  (rainy season;  $R^2 = 0.95$ ),  $\delta^2\text{H} = 4.6 \cdot \delta^{18}\text{O} - 20.7$  (dry season;  $R^2 = 0.74$ ). This signature aligns with expectations for surface water bodies, where open exposure facilitates fractionation. The box plot confirms strong evaporative enrichment, with median values shifted significantly toward more



462 positive  $\delta^{18}\text{O}$  and  $\delta^2\text{H}$  compared to rainfall (Fig. 6a, c). Pond water maintains a relatively consistent slope  
 463 and range across seasons, reinforcing its stable evaporative signature and less dynamic recharge behavior.

464 Spring water shows a clear seasonal transition in its isotopic composition. In the rainy season, its  
 465 evaporation line ( $\delta^2\text{H} = 6.2 \cdot \delta^{18}\text{O} - 11.4$ ;  $R^2 = 0.75$ ) falls closer to the LMWL, suggesting that spring  
 466 discharge is augmented by recent rainfall, likely delivered through rapid infiltration and shallow  
 467 subsurface flow pathways during high-intensity events (Fig. 6a, b). However, the isotopic values of  
 468 spring water are substantially more depleted than those of precipitation, indicating that older water stored  
 469 in the porous subsurface aquifer dominates the overall spring flow composition composed of new and  
 470 relatively old water.

471 During the dry season, the isotopic slope flattens and deviates further from the Local Meteoric Water  
 472 Line (LMWL), reflecting increased evaporative influence or prolonged residence times (Fig. 6c, d). This  
 473 seasonal shift suggests that as rainfall inputs decline, spring discharge becomes increasingly composed  
 474 of slow-draining, older water that has undergone greater isotopic modification—either through mixing  
 475 or evaporation in near-surface storage zones. Collectively, these patterns suggest that spring water acts  
 476 as a dynamic integrator of recharge processes—rapidly responding to event-driven infiltration during the  
 477 rainy season, yet also reflecting the delayed mobilization of older water stored in the subsurface. This  
 478 behavior may be partly explained by a piston-like displacement mechanism, where incoming rainfall  
 479 pushes pre-existing groundwater toward discharge zones.

480 Pore and fissure water show remarkably similar isotopic signatures during the rainy season. Pore  
 481 water, again sampled from a porous subsurface aquifer, follows a fitted line of  $\delta^2\text{H} = 4.3 \cdot \delta^{18}\text{O} - 27.9$   
 482 (rainy season;  $R^2 = 0.74$ ), while fissure water, likely drawing from the same aquifer but through  
 483 weathered bedrock pathways, fits  $\delta^2\text{H} = 3.7 \cdot \delta^{18}\text{O} - 32.0$  (rainy season;  $R^2 = 0.70$ ). These slopes are  
 484 significantly flatter than those of rainfall, pond, or spring water, a pattern interpreted as evidence of  
 485 evaporation prior to recharge or mixing with evaporated surface water. However, the box plots of the  
 486 isotope data present a different picture. Both pore and fissure waters are systematically more depleted in  
 487  $\delta^{18}\text{O}$  and  $\delta^2\text{H}$  than precipitation, and their narrow interquartile ranges suggest a relatively uniform  
 488 isotopic composition (Fig. 6a-d). Rather than showing the enrichment expected from evaporation, these  
 489 depleted and stable values point toward recharge dominated by a limited number of isotopically light  
 490 rainfall events, such as early-season storms or high-altitude convective systems.

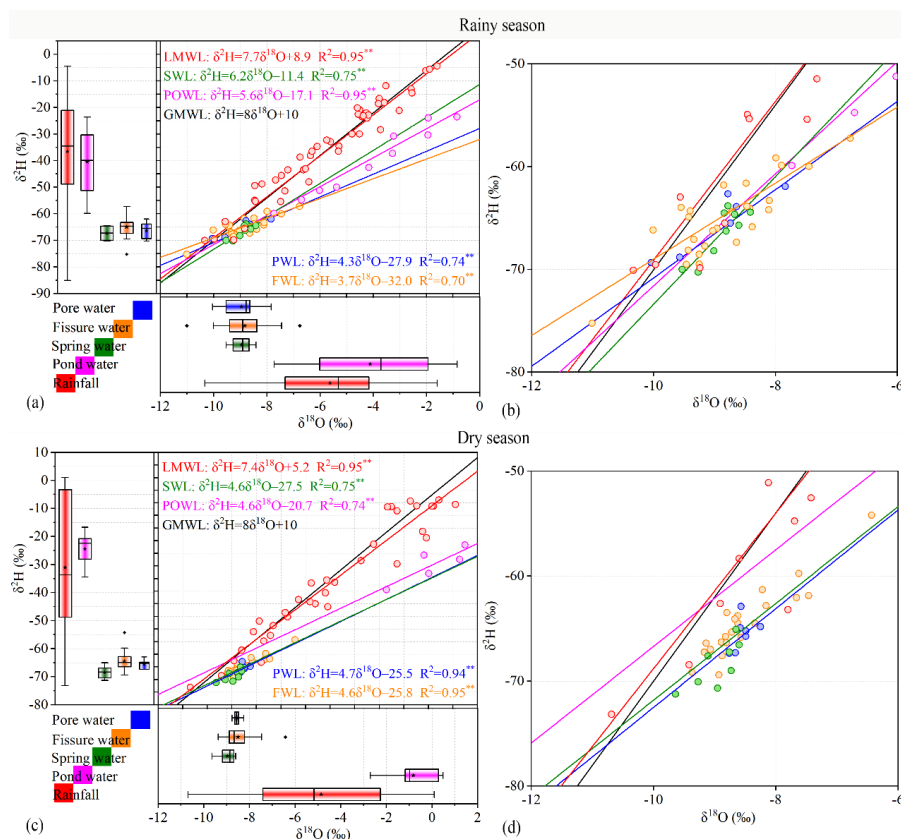


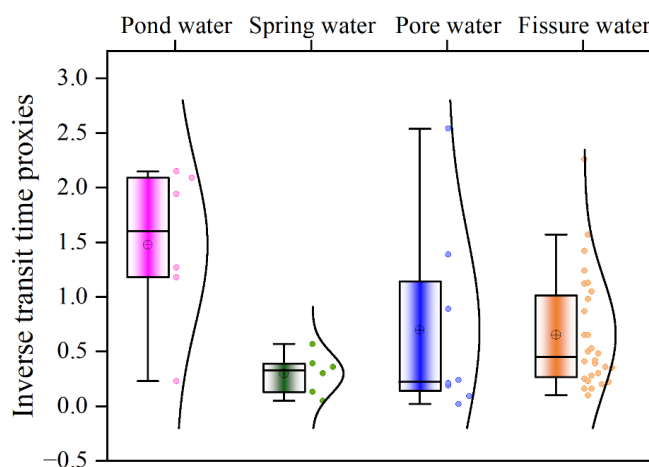
Fig. 6. Dual stable isotopic compositions of rainfall, pond water, spring water, pore water, and fissure water during the (a) rainy season and (b) dry season in the gully region of the Loess Plateau. The black line represents the global meteoric water line (GMWL,  $\delta^2\text{H}=10 + 8\delta^{18}\text{O}$ ). GMWL is the global meteoric water line of Craig, LMWL is the local meteoric water line, SWL is the spring water line, POWL is the pond water line, FWL is the fissure water line, and PWL is the pore water line. Panels (b) and (d) are magnified views of (a) and (c), respectively, highlighting the isotopic compositions of pore water, fissure water, and spring water (x-axis:  $-12$  to  $-6\text{‰}$ ; y-axis:  $-80$  to  $-50\text{‰}$ ).

This apparent contradiction—flat regression slopes alongside depleted and uniform isotopic compositions—can be reconciled by considering longer residence times and mixing in the subsurface. The aquifer likely functions as a hydrological buffer, smoothing short-term isotopic variability and maintaining a signature reflective of older recharge. In this context, the low slopes may not indicate evaporation but instead reflect the dampening of seasonal isotope fluctuations through storage and subsurface mixing (Table A2).



505 Complimenting the isotope data,  $\text{Cl}^-$  levels in pore water consistently fall between those of  
 506 precipitation and pond water across both seasons (Fig. A2), supporting a mixed recharge origin. This  
 507 trend aligns with the isotopic evidence from the rainy season and supports the interpretation that pond  
 508 water contributes to pore water recharge via vertical percolation through the vadose zone, particularly  
 509 during high-rainfall periods when infiltration capacity is exceeded. The lack of a similar isotopic pattern  
 510 in the dry season likely reflects stronger evaporative enrichment of pond water, which masks its potential  
 511 contribution to pore water recharge in dual-isotope space.

512 The inverse transit time proxies (ITTPs) broadly support the dual-isotope interpretations of water  
 513 source dynamics. Pond water exhibited the highest ITTP values ( $1.5 \pm 0.7$ ), indicating rapid turnover and  
 514 limited subsurface storage. These elevated values likely reflect inputs from direct rainfall and overland  
 515 flow, as well as evaporative enrichment, which increases isotopic variability and can artificially shorten  
 516 the apparent residence time. In contrast, pore water ( $0.7 \pm 0.3$ ) and fissure water ( $0.6 \pm 0.5$ ) showed lower  
 517 ITTPs, consistent with longer residence times, greater subsurface mixing, and attenuation of seasonal  
 518 isotopic signals due to delayed recharge. Spring water had the lowest ITTPs ( $0.3 \pm 0.2$ ), reflecting slow  
 519 subsurface transport and integration of older water sources. While these patterns align with conceptual  
 520 expectations of residence time and flow path length, the limited number of samples—particularly for  
 521 pond, spring, and pore water—warrants caution in interpreting seasonal dynamics (Fig. 7).



522  
 523 Fig. 7. Boxplots and kernel density estimates of inverse transit time proxies (ITTPs) for pond water,  
 524 spring water, pore water, and fissure water. Higher ITTP values indicate shorter water transit times since  
 525 precipitation, while lower values suggest longer residence and greater isotopic damping. Pond water



526 exhibited the highest and most consistent ITTPs (median  $\approx 1.5$ ), implying rapid recharge from recent  
 527 rainfall or stormflow. Spring water showed the lowest ITTPs ( $\approx 0.3$ ), consistent with longer subsurface  
 528 flow paths and storage. Pore and fissure water displayed intermediate and more variable ITTPs, reflecting  
 529 mixing between recent and older water sources, as well as seasonal differences in infiltration and soil  
 530 moisture replenishment.

531

### 532 **5.3. Hydrological linkages and recharge efficiency**

533 The SEM analysis reveals significant hydrological linkages among different water bodies in the  
 534 catchment, with particularly well-defined pathways connecting rainfall, pond water, pore water, and  
 535 fissure water (Fig. 8a, b). Several key pathways identified in the model are supported by multiple lines  
 536 of observational evidence, including isotopic composition, chloride concentrations, and water age (ITTP).  
 537 Rainfall contributes over 73% to pore water recharge, far exceeding the  $<17\%$  contribution from pond  
 538 water (Fig. 8c).

539 However, the SEM results indicate that the total effect of pond water on pore water is stronger than  
 540 that of rainfall (Fig. 8b). In SEM, the total effect includes both direct pathways (e.g., pond water  $\rightarrow$  pore  
 541 water) and indirect pathways mediated by other variables (e.g., rainfall  $\rightarrow$  pond water  $\rightarrow$  pore water).  
 542 This apparent contradiction likely stems from the strong statistical association between rainfall and pond  
 543 water, as pond water is primarily derived from rainfall and shares similar isotopic signatures. As a result,  
 544 the model may overestimate pond water's influence on pore water due to overlapping signals and  
 545 correlated pathways.

546 These findings underscore the importance of integrating multiple lines of evidence rather than  
 547 relying solely on SEM outputs. For example, chloride concentrations in pore water more closely resemble  
 548 those of pond water, suggesting mixed recharge from both sources and highlighting the potential for pond  
 549 water to play a prominent role under certain spatial or temporal conditions (Fig. 2a). Although dry-season  
 550 isotopic data provide limited support for a strong pond water–pore water connection, the spatial  
 551 distribution of chloride offers compelling evidence that pond water can contribute significantly to pore  
 552 water recharge, particularly in localized areas or during specific recharge events.

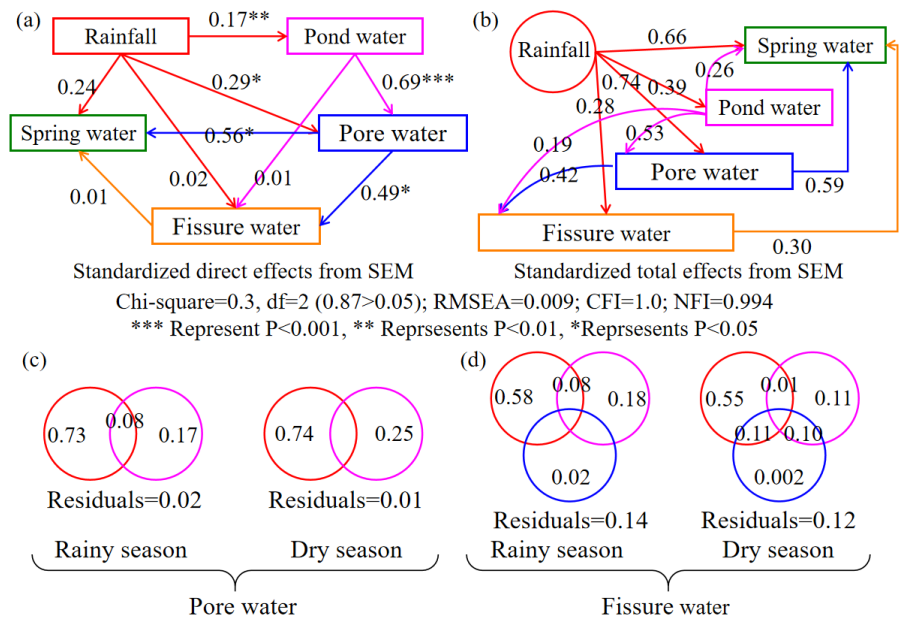
553 At deeper levels, the linkage between pore water and fissure water is supported by their nearly  
 554 identical isotope values and similar ITTPs, suggesting a shared subsurface origin and a strong  
 555 hydrological connection (Fig. 8a, b). In contrast, although there is some hydrological connectivity





556 between pore water and spring water, differences in isotopic slopes and residence times may lead to an  
557 overestimation of their interaction. However, their nearly identical chloride concentrations provide more  
558 direct and reliable evidence of connectivity.

559 Although the model results initially suggest that rainfall—mediated through pond water—is the  
560 primary source of pore water recharge, discrepancies among the different indicators call for a more  
561 critical interpretation of the evidence. The contradictions observed across isotopic, chloride, and ITTP  
562 data underscore the need for further quantitative validation.



563  
564 Fig. 8. Structural equation modeling (SEM) and variance partitioning results illustrating hydraulic  
565 connectivity among water sources in the gully region of the Loess Plateau. Panels (a) and (b) show the  
566 standardized direct (a) and total effects (b) among rainfall, pond water, pore water, spring water, and  
567 fissure water, based on  $\delta^{18}\text{O}$  and  $\delta^2\text{H}$  data. Arrows indicate hypothesized water flow pathways, with line  
568 thickness proportional to effect size. Asterisks denote statistical significance ( $*P<0.05$ ,  $**P<0.01$ ,  
569  $***P<0.001$ ). The model fit is excellent ( $\chi^2=0.3$ ,  $df=2$ ,  $RMSEA=0.009$ ,  $CFI=1.0$ ,  $NFI=0.994$ ),  
570 supporting the robustness of these inferred connections. Panels (c) and (d) present variance partitioning  
571 results showing the relative contributions of source waters to pore water and fissure water during the  
572 rainy and dry seasons, respectively. In panel (c), rainfall (red) and pond water (pink) explain a large  
573 portion of pore water variability, with some shared explanatory power and modest residuals. In panel (d),



574 fissure water reflects a more complex origin, with contributions from rainfall (red), pond water (pink),  
575 and pore water (blue), and greater overlap and residuals, especially during the dry season.

576 To address the contradictions observed in the SEM and variance partitioning results, we apply the  
577 water table fluctuation method to independently estimate the recharge rate from rainfall to pore water.  
578 Groundwater level fluctuations in the gully system revealed clear seasonal recharge dynamics, with an  
579 initial rise in the pore water table beginning on October 24, 2023, followed by a decline through early  
580 spring (March 1, 2024) and a gradual recovery starting June 20, 2024 (Fig. 9a). Between October 24,  
581 2023, and October 24, 2024, cumulative recharge was estimated at  $238.0 \pm 6.0$  mm (RISE) and  
582  $241.4 \pm 6.0$  mm (MRC), with 159 and 167 recharge days, respectively (Fig. 9b). Given that annual  
583 precipitation totaled approximately 550 mm, recharge efficiency was approximately 43–44%,  
584 underscoring the significance of focused infiltration in sustaining shallow aquifer recharge within the  
585 gully environment.

586 This recharge efficiency is lower than the precipitation-to-pore water contribution estimated by the  
587 variance decomposition method and may more accurately reflect “actual” recharge, as statistical  
588 estimates can be biased by similarities in isotopic signatures. When integrated with dual-isotope and  
589 SEM analyses, the WTF-based results support a conceptual model in which storm-driven runoff is  
590 efficiently captured and redistributed through loess soil matrices and retention structures (e.g., ponds,  
591 check dams), activating a hierarchy of shallow and deeper subsurface flowpaths. These flowpaths link  
592 pore water, fissure water, and spring discharge across the complex gully landscape, reflecting both  
593 vertical and lateral connectivity within the groundwater system.

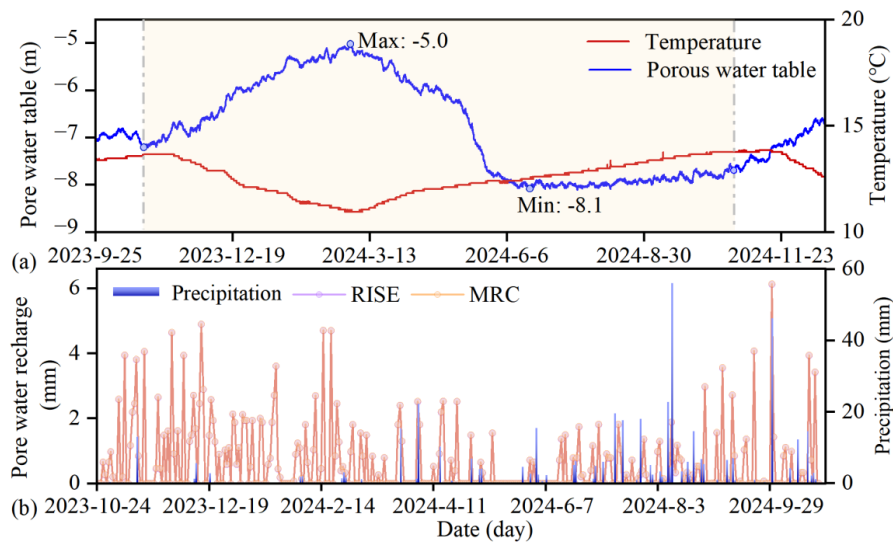


Fig. 9. Temporal dynamics of pore water table depth, temperature, precipitation, and recharge in the gully region of the Loess Plateau. (a) Daily time series of pore water table depth (blue line) and surface temperature (red line) from September 2023 to November 2024. The water table fluctuates seasonally, rising from  $\sim -8.1$  m in late summer to a maximum of  $\sim -5.0$  m in early spring (March 2024), indicating delayed infiltration and cool-season recharge. (b) Daily precipitation (blue bars) and modeled pore water recharge estimates using the RISE and MRC methods. Most recharge events occur from October to April, even when rainfall is not especially high, while warm-season precipitation contributes little to recharge—likely due to increased evaporative losses and shallow soil retention. Together, these patterns suggest strong seasonal control on recharge processes, with effective infiltration primarily occurring during cooler, low-evaporation periods.

## 6. Discussion

### 6.1. Isotopic compositions of various water bodies in the gully region

In hydrological studies, the isotopic composition of water bodies reflects both sources and changes in hydrological processes (Wan and Liu, 2016; Kumar et al., 2019; Dasgupta et al., 2024). Precipitation, surface water, and groundwater usually exhibit differences in isotopic characteristics due to variations in evaporation, infiltration, and mixing (Gleeson et al., 2016; Kuang et al., 2019; Al-Oqaili et al., 2020). However, similar isotopic distributions among different water bodies often indicate a strong hydrological



613 connection in their water sources (Yang and Wang, 2023).

614 Our study found that rainfall and pond water have similar spatial isotopic distribution patterns,  
 615 indicating that pond water primarily originates from rainfall. This reflects the region's geographical and  
 616 hydrological characteristics. In this severely eroded gully region, the local government has constructed  
 617 an extensive network of ponds and check dams to capture hillside runoff (Liu et al., 2017; Xue et al.,  
 618 2025). As a result, most precipitation from the hills converges into these gully ponds and check dams. A  
 619 lower pond water line slope indicates evaporation fractionation during retention. Evaporation  
 620 preferentially removes lighter isotopes ( $^1\text{H}$  and  $^{16}\text{O}$ ), enriching heavier isotopes ( $^2\text{H}$  and  $^{18}\text{O}$ ) and shifting  
 621 the pond water's isotopic composition from its precipitation source (Aragu et al., 1998; Zhang and Wu,  
 622 2009; Gleeson et al., 2016). This similarity is primarily due to the fact that pond water originates from  
 623 rainfall and its runoff in the hilly-gully region (Liu et al., 2011; Ji et al., 2024). Additionally, the isotopic  
 624 values of most groundwater in the gully areas are more depleted compared to those of rainfall and pond  
 625 water, likely due to the recharge mechanisms and residence times of the different groundwater types  
 626 (Ouali et al., 2024). Nevertheless, these values fall within the range of precipitation isotopic values,  
 627 leaning towards the more negative end, suggesting that groundwater is likely directly recharged by  
 628 significant precipitation events. This is due to the thin unsaturated zone (<10 m) in the gully areas, which  
 629 facilitates rapid infiltration and direct recharge from heavy rainfall.

630 To further investigate the complexity of different types of groundwater in the gully area, we  
 631 conducted hydrological and geological surveys, collecting water samples from spring water, pore water,  
 632 and fissure water. The results show that the isotopic values of spring water, pore water, and fissure water  
 633 are closely clustered, indicating a strong interconnection among the different types of groundwater within  
 634 the hydrological cycle. This is likely due to their shared geological and hydrological environments  
 635 (Bouwer, 2002; Li et al., 2021; Zhang et al., 2022). Our study found that the water line slope of pore  
 636 water and fissure water was higher in the dry season than in the rainy season, with values falling between  
 637 the slopes of pond water from the rainy and dry seasons. To investigate the cause of these results, we  
 638 analyzed groundwater level dynamics, which showed that water tables were lower at the end of the rainy  
 639 season but rebounded afterward, making dry-season tables higher. This suggests that rainy-season  
 640 groundwater mixes with evaporatively enriched water, lowering its slope, while dry-season groundwater  
 641 is recharged by delayed rainfall and pond water, increasing its slope. These findings reveal that isotopic  
 642 composition is influenced by both current and prior hydrological conditions. They also highlight the



643 complexity of evaporation fractionation regulated by water mixing and demonstrate the significant  
 644 impact of pond construction on groundwater recharge and regional hydrology in the gully regions.

645

## 646 **6.2. Groundwater recharge processes in the gully region**

647 In recent years, discussions of groundwater recharge sources have primarily focused on tableland  
 648 and hilly areas with thick loess deposits, although only a few researchers have examined gully regions  
 649 (Li et al., 2017; Xiang, 2020; Lu, 2020). For example, Liu et al. (2011) found that groundwater near  
 650 valleys in the hilly loess area is replenished by precipitation, runoff, and surface water. Our findings  
 651 support this study, identifying rainfall and surface water as major sources of gully groundwater recharge.  
 652 We classify groundwater into three types (spring water, pore water, and fissure water) and propose a  
 653 gradual recharge process, including (1) direct and indirect recharge from precipitation to pond water and  
 654 pore water, respectively; (2) concentrated recharge from pond water to pore water; and (3) percolation  
 655 recharge from pore water to fissure water. This reflects the complexity of the groundwater system and  
 656 the significant impact of human activities (e.g., ponds and check dams) on hydrological processes.

657 In the deep-profile unsaturated zones of the hilly region on the Loess Plateau, previous studies have  
 658 used chloride mass balance and tritium peak methods to estimate groundwater recharge from  
 659 precipitation, typically accounting for 2%–22% of annual rainfall, with water residence times in the  
 660 unsaturated zone lasting several years or even hundreds of years (Huang et al., 2011; Tan et al., 2016; Li  
 661 et al., 2017; Wang et al., 2024). However, these studies did not address the catchment role of gully regions.  
 662 Field observations and past studies show that precipitation rarely directly infiltrates thick loess in hilly  
 663 areas (Xu et al., 1993; Li, 2001). Instead, it forms surface runoff that converges into gullies and  
 664 accumulates in ponds or other water bodies (perched water), serving as a concentrated recharge source  
 665 for groundwater (Yu et al., 2025), reflecting the sustained and delayed impact of gully runoff on  
 666 groundwater recharge, which is consistent with the results of this study.

667 Notably, our study does not consider confined water. Tan et al. (2016) indicated that the groundwater  
 668 in the high mountain-hilly loess aquifer does not originate from the upwelling of ancient regional  
 669 groundwater, and there is no evidence of deep confined water beneath the loess strata in the high  
 670 mountain-hills. Additionally, our findings represent only the groundwater recharge results in the gully  
 671 regions for two reasons: 1) The hydrological system is complex, with significant variations across  
 672 different landscapes of the Loess Plateau (Li et al., 2019; Li et al., 2021). For example, Li et al. (2019)



673 found that groundwater dominates the hydrological system in the tableland on the Loess Plateau, where  
674 surface water (streams) is recharged by groundwater because river channels are deeper than the bedrock.  
675 2) Our data collection focused on gully because the “Loess Liang” and “Loess Mao” hillside areas are  
676 covered by thick loess with minimal water sources.

677

### 678 **6.3. Groundwater recharge rates in the gully region**

679 In many parts of the world, identifying the sources of groundwater recharge and its renewability is  
680 essential for effective water resource management (Ajjur and Baalousha, 2021; Meles et al., 2024). In  
681 the hilly-gully region of the Loess Plateau, where groundwater is considered a crucial source of safe  
682 water, understanding the origins and recharge of aquifers provides valuable information for water  
683 resource planners (Liu et al., 2011; Wang et al., 2024). This knowledge is essential and should be shared  
684 with regions facing similar challenges.

685 Groundwater recharge can be quantified from three hydrological sources: surface water, the  
686 unsaturated zone, and the saturated zone (Scanlon et al., 2022). Recharge estimates based on the saturated  
687 zone are generally more reliable than those from the unsaturated zone, as the latter represents potential  
688 recharge that may not ultimately reach the groundwater table (Beven and Germann, 2013; Huang et al.,  
689 2019). The groundwater table fluctuation method is widely used for estimating saturated zone recharge  
690 due to its high temporal resolution and intuitive nature (Gumuła-Kawęcka et al., 2022; Xu et al., 2024).  
691 In our study area, ITTPs estimated similar transit times for both pore water and fissure water. Therefore,  
692 we used the groundwater table fluctuation method to assess the recharge of pore water in the gully region.  
693 The total recharge from 2023 to 2024 was estimated at  $241.4 \pm 6.0$  mm and  $238 \pm 6.0$  mm using the MRC  
694 and RISE methods, respectively. Under constant specific yield conditions, the MRC method typically  
695 estimates higher groundwater recharge and recharge days than RISE, as it accounts for groundwater table  
696 decline due to lateral outflow and other discharge processes in the absence of recharge (Heppner and  
697 Nimmo, 2005). Our findings support this pattern. Furthermore, the key parameter for estimating  
698 groundwater recharge using the groundwater table fluctuation method is specific yield, which depends  
699 on factors such as soil properties and water table depth. This value can be derived from empirical soil  
700 texture, pumping tests, or the test pit method (Nachabe, 2002; Liang et al., 2016). Shah and Ross (2009)  
701 found the test pit method reliable for water tables deeper than 2 m. In this study, with a water table  
702 exceeding 2 m, the specific yield was 0.32, consistent with values of 0.3 in similar soil conditions (Wang



703 et al., 2023).

704 Research on groundwater recharge in the Loess Plateau has mainly focused on deep-profile  
 705 unsaturated zones in the tableland and hilly areas, with tracer methods estimating recharge between 9 to  
 706 100 mm (Huang et al., 2011; Li et al., 2017; Lu, 2020; Wang et al., 2024). In contrast, our study in the  
 707 gully region indicates recharge of up to 240 mm, much higher than previous estimates on deep-profile  
 708 unsaturated zones. This difference reflects several factors: 1) Unsaturated zone thickness—In the gully  
 709 region, the unsaturated zone is generally less than 10 m thick, much shallower than in tableland and hilly  
 710 areas (mean thickness of 92.2 m), making infiltration easier and promoting effective recharge. 2) Gully  
 711 topography and hydrology—characterized by well-developed channels, concentrated runoff, and  
 712 widespread ponds and check dams—promote focused infiltration (Liu et al., 2017; Li et al., 2021; Xue  
 713 et al., 2025). 3) Research methods—Tracer methods reflect long-term recharge rates and are better suited  
 714 for thicker unsaturated zones (Huang et al., 2011; Lu, 2020; Li et al., 2017). In contrast, the water table  
 715 fluctuation method directly captures short-term recharge dynamics and works better in thinner  
 716 unsaturated zones. Moreover, this method also better captures surface water-groundwater interactions  
 717 and focused recharge effects (Gumuła-Kawęcka et al., 2022). These findings underscore the importance  
 718 of studying recharge in gully regions, filling a research gap in the Loess Plateau's geomorphology and  
 719 providing new ecohydrological insights. Furthermore, our study demonstrates the potential of artificial  
 720 ponds to regulate water resources and enhance recharge, with valuable implications for water  
 721 management and ecological engineering.

722

#### 723 **6.4. Revised conceptual model**

724 To convey our evolving understanding of the spatial structure and dynamics in the Gully Region,  
 725 we developed a conceptual model that reframes gullies not simply as erosion features but as active  
 726 hydrological conduits for groundwater recharge (Fig. 10). This model integrates stable isotope signatures,  
 727 variations in chloride concentrations, ITTPs, groundwater level dynamics, and soil physical properties  
 728 such as porosity and field water capacity. Through this integrative framework, we elucidate the  
 729 transformation of precipitation into various forms of subsurface water by explicitly tracing its movement  
 730 through a cascade of compartments—from surface ponding in dammed gullies, to infiltration through the  
 731 unsaturated zone, and eventual recharge into both the porous aquifer and underlying bedrock fissure  
 732 systems.





733 This conceptual reframing is grounded in the stark hydrological contrasts between hilly uplands and  
734 gully systems and directly addresses a critical knowledge gap in understanding the hydrological  
735 functioning of gully environments. In the hilly uplands, thick loess deposits—often exceeding 90 m  
736 (including low-permeability aquifers)—combined with steep slopes ( $>15^\circ$ ) severely restrict vertical  
737 infiltration. Compounded by short-duration, high-intensity rainfall events that provide insufficient  
738 moisture for deep profile wetting, this results in the rapid conversion of rainfall into surface runoff (Li et  
739 al., 2021; Zhu et al., 2018). This runoff is systematically funneled downslope into gully systems, a  
740 process further intensified by engineered interventions such as check dams and retention ponds that  
741 intercept and concentrate overland flow. Because precipitation seldom infiltrates directly into the thick  
742 loess of upland regions (Xu et al., 1993; Li, 2001), most infiltration occurs after surface water  
743 accumulates in gullies—particularly within perched water bodies like ponds—which subsequently serve  
744 as focal points for groundwater recharge (Yu et al., 2025).

745 Crucially, gully systems possess distinct hydrogeological characteristics: the loess mantle is much  
746 thinner (typically  $< 25$  m), and the soils are dominated by silt loam textures with moderate specific yield  
747 (0.02–0.05) and high field capacity (21–28%). These properties promote transient water storage and  
748 enable temporally delayed, depth-partitioned infiltration. Based on our integrated analyses of stable  
749 isotopes, chloride concentrations, and inverse transit time proxies, we find that gullies function not as  
750 passive erosional features but as active recharge conduits. This conceptualization captures a critical  
751 spatial transition—from runoff generation in the hilly uplands to focused recharge in gully zones—  
752 emphasizing the pivotal role of gully systems in regulating groundwater recharge across the Loess  
753 Plateau landscape.

754 Combined hydrological monitoring and multi-indicator analysis further reveal that following the  
755 rainy season, infiltration depths on hilly slopes are typically shallow—less than 1 m—while groundwater  
756 levels in gully areas exhibit pronounced rises exceeding 2 m. Recharge estimates based on the water table  
757 fluctuations reach up to 240 mm, far surpassing values observed in deep unsaturated zones of tablelands  
758 and hills (Huang et al., 2011; Li et al., 2017; Lu, 2020; Wang et al., 2024). These results reinforce the  
759 role of gullies as focal points for groundwater recharge and are consistent with prior studies. For instance,  
760 in hilly areas, precipitation rarely recharges groundwater due to the thick loess layers, with an average  
761 infiltration depth of only 1 meter (Wang et al., 2024).

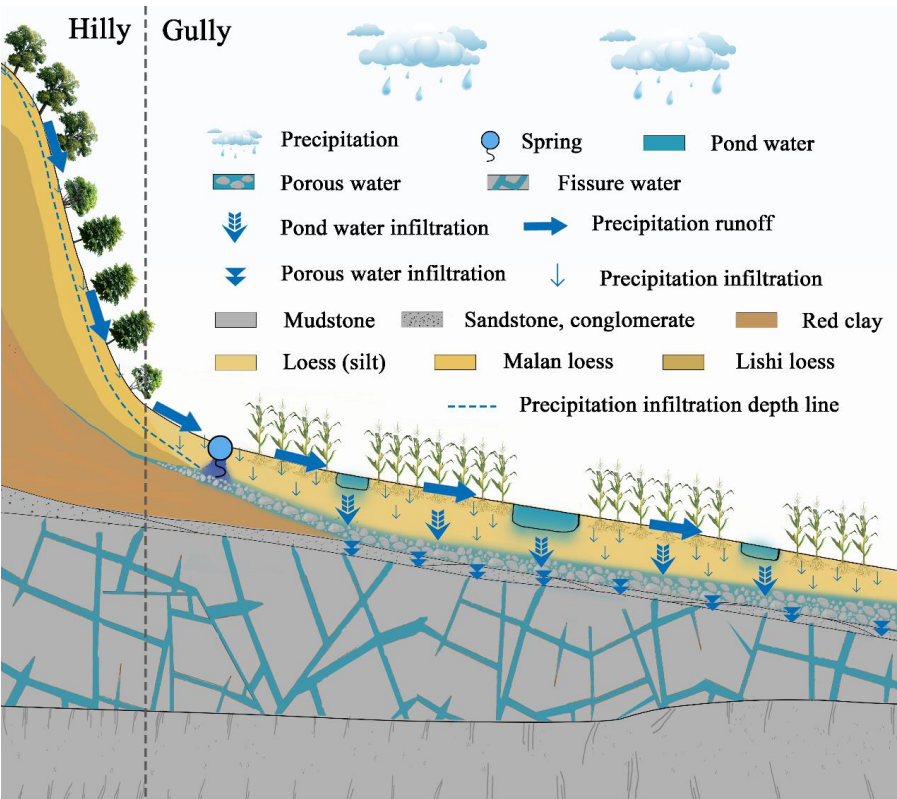
762 Liu et al. (2011) found that groundwater near valleys in the hilly loess area is replenished by



763 precipitation, runoff, and surface water. Moreover, fissure water exhibits more depleted isotopic  
764 signatures and higher chloride concentrations, indicating deeper percolation of pore water or mixing with  
765 older recharge sources. These patterns, supported by ITTPs and partial SEM linkages, reveal a  
766 hierarchical recharge sequence: event-driven infiltration enters the shallow pore aquifer, some of which  
767 slowly percolates into deeper fissure zones. This hierarchical mechanism is facilitated by the combination  
768 of thin loess mantles, engineered interventions (e.g., check dams and ponds), and delayed hydrological  
769 responses.

770 By integrating multiple lines of evidence, this conceptual model redefines gullies as selective  
771 recharge corridors shaped by both geomorphic structure and human intervention. It challenges the  
772 traditional view of gullies as purely erosional landforms and emphasizes their dual hydrological function:  
773 acting both as runoff conveyance channels and as transient reservoirs that store and redistribute water  
774 across space and time. This recharge capacity is jointly governed by topographic convergence, reduced  
775 loess thickness, and the presence of engineered structures such as check dams and retention ponds.

776 Crucially, the model offers insight into the multifunctionality of ecological engineering—  
777 particularly check dams and ponds—in enhancing hydrological regulation, water security, and ecosystem  
778 restoration across the Loess Plateau. Compared to the traditional piston-flow and preferential flow  
779 models commonly applied in the region, the proposed “gully-dominated preferential recharge mechanism”  
780 marks a notable theoretical advancement. Whereas previous models primarily emphasize vertical  
781 infiltration through homogeneous loess layers, this study is the first to quantitatively identify a cascade  
782 recharge process unique to thin-loess gully catchments. By identifying the pivotal role of gully systems  
783 in stormwater detention, delayed infiltration, and multi-aquifer recharge, this study establishes a robust  
784 theoretical and technical foundation for improving water resource allocation, infrastructure planning, and  
785 groundwater sustainability in arid and semi-arid regions. Beyond advancing theoretical understanding of  
786 regional hydrological processes, it also provides a sound basis for developing spatially targeted models  
787 of groundwater recharge.



788  
789 Fig. 10. Hydraulic connections between different water bodies in the hilly-gully region of the Loess  
790 Plateau. The study area consists of hilly and gully regions. In the hilly area, the stratigraphic sequence  
791 from top to bottom is Malan loess, Lishi loess, red clay, sandstone, and mudstone. Rainfall infiltration  
792 within the Malan loess is less than 1 m, and the area is mainly covered by vegetation. In the gully area,  
793 the stratigraphy from top to bottom includes loess (silt), sandstone and conglomerate, and mudstone.  
794 Pore water is found within the sandstone and conglomerate, while fissure water occurs in bedrock  
795 fractures (mudstone). Numerous check dams or ponds are distributed throughout the gully area. The  
796 vertical separation between the pore water and pond water ranges from 3 to 5 m. Corn is the main crop  
797 cultivated in this region. Most springs in the study area are located at the junction of the hilly and gully  
798 regions and are discharged from pore water.

799  
800 **6.5. Limitations and future research directions**

801 This study underscores the limitations of relying on a single indicator to infer groundwater recharge  
802 pathways, as doing so may lead to oversimplified or potentially misleading interpretations of complex



803 hydrological processes. While stable isotope signatures confirm that precipitation contributes to pore  
804 aquifer recharge, they do not provide clear evidence of direct recharge from pond water to either pore or  
805 fissure groundwater during the dry season. In contrast, the spatial distribution of chloride concentrations  
806 offers compelling support for focused pond water leakage into the shallow groundwater system.

807       Although variance decomposition analysis and structural equation modeling suggest statistical  
808 linkages among different water bodies and provide useful clues about potential recharge pathways, these  
809 associations may be confounded by overlapping isotopic signatures or by non-conservative processes  
810 such as evaporation and mixing, potentially leading to an overestimation of hydrological connectivity. In  
811 the absence of mass balance constraints, the pathways inferred through SEM may not accurately reflect  
812 the actual flow processes within the groundwater system. By contrast, the water table fluctuation method  
813 captures both vertical and lateral recharge processes, yielding estimates that are more likely to reflect  
814 actual recharge rates. Drawing on this empirical evidence, the present study further substantiates the  
815 critical role of gully zones in regional groundwater recharge.

816       Despite effort to address uncertainties, limitations remain in terms of spatial and temporal sampling  
817 density. For example, the lack of long-term tracers such as groundwater age, combined with limited  
818 observations of groundwater level fluctuations, constrains our ability to assess recharge dynamics over  
819 multi-year timescales. Additionally, the current sampling design includes only two campaigns during the  
820 rainy and dry seasons, which may be insufficient to fully capture the seasonal variability of ITTP values.  
821 This, in turn, may affect the accuracy of groundwater renewal frequency estimates and the strength of  
822 inferred hydrological connections. In arid and semi-arid regions, groundwater recharge is typically  
823 triggered by infrequent, high-intensity rainfall events. However, existing sampling strategies based on  
824 seasonal intervals often lack the temporal resolution necessary to capture these short-lived, event-driven  
825 recharge processes effectively.

826       Future research should address these issues through several improvements: (1) conducting higher-  
827 frequency, event-scale sampling to systematically monitor rainfall, spring discharge, and pond water  
828 level dynamics, thus capturing the influence of key hydrological events on recharge processes; (2)  
829 expanding the spatial coverage of pore and fissure well monitoring to improve the accuracy of regional  
830 recharge pattern identification; and (3) incorporating additional environmental tracers (e.g.,  $^3\text{H}$ ,  $^{22}\text{Na}$ ) to  
831 trace flow paths and estimate recharge lag times. In addition, systematic observation of event-scale  
832 hydrological processes should be strengthened by establishing a high-frequency, event-driven monitoring



833 network to better capture the nonlinear coupling among rainfall, surface runoff, and groundwater  
834 dynamics. This approach would significantly improve our understanding of rapid infiltration events and  
835 associated recharge mechanisms.

836 From a methodological perspective, integrating statistical techniques—such as SEM and variance  
837 decomposition analysis—with process-based physical models like MODFLOW and HYDRUS can  
838 provide mechanistically constrained insights into recharge pathways. Compared to correlation-based  
839 statistical methods, physical models offer greater precision in characterizing groundwater flow and  
840 recharge processes across both temporal and spatial dimensions, helping to reduce uncertainties  
841 associated with non-conservative tracer behavior and the absence of mass balance constraints. Regarding  
842 measurements, hydrometric instrumentation within check dams and beneath pond beds could further  
843 quantify the recharge effects of various engineering interventions under specific hydrological conditions.  
844 Additionally, integrating isotopic data with mean transit time modeling, combined with targeted field  
845 monitoring and improved spatial analysis, could help elucidate recharge pathways, quantify temporal  
846 dynamics, and enhance process-level understanding of groundwater recharge in complex dryland  
847 landscapes. Collectively, these efforts will contribute to a stronger theoretical foundation and offer  
848 practical guidance for the precise management of water resources, the design of ecologically appropriate  
849 engineering interventions, and the implementation of effective landscape rehabilitation strategies.

850

## 851 7. Conclusion

852 Through integrated analysis of stable isotopes, chloride concentrations, water table fluctuations, and  
853 inverse transit time proxies, we developed multiple lines of evidence to reframe gullies in the Loess  
854 Plateau as hydrologically significant recharge zones, rather than solely as indicators of erosion and  
855 degradation. Precipitation events drive substantial recharge to shallow pore aquifers, with annual rates  
856 exceeding 238 mm—accounting for a large fraction of annual rainfall. While isotopic evidence for  
857 recharge from pond water is obscured by evaporative fractionation, chloride concentrations provide a  
858 clear signal of subsurface connectivity. Recharge in this system is both spatially concentrated and  
859 temporally selective, shaped by terrain configuration, loess stratigraphy, and ecological engineering  
860 structures such as check dams and ponds.

861 These findings offer a process-based foundation for developing hydrological indicators of landscape  
862 function and restoration performance in dryland environments. Specifically, recharge magnitude, isotopic



damping, and solute accumulation patterns may serve as diagnostic tools for identifying effective recharge zones and tracking system responses to intervention. To refine these indicators, future studies should incorporate high-frequency monitoring, event-based sampling, and multi-tracer approaches. Collectively, this work challenges conventional views of gullies as hydrological liabilities and demonstrates their underappreciated role as targeted recharge assets—advancing dryland groundwater sustainability and providing actionable insights for landscape-scale ecological restoration and management.

870

871

872

**Author contributions:**

ZXJ: Conceptualization, Methodology, Formal analysis, Investigation, Visualization, Data curation, Validation, Writing-original draft. ADZ: Conceptualization, Formal analysis, Validation, Visualization, Writing-review & editing. LW: Conceptualization, Funding acquisition, Project administration, Resources, Supervision, Visualization, Writing-review & editing.

**Data availability:**

Data are available from the corresponding author upon reasonable request.

**Conflicts of Interest:**

The contact author has declared that none of the authors has any competing interests.

**Acknowledgments:**

This work was supported by the National Natural Science Foundation of China (grant numbers 42171043, 42377318, and U24A20629).

885

886

887

888

889



## 890 References

- 891 Ajjur, S.B., Baalousha, H.M. A review on implementing managed aquifer recharge in the Middle East  
 892 and North Africa region: methods, progress and challenges. *Water International*. 46(4): 578-604, 2021.  
 893 <https://doi.org/10.1080/02508060.2021.1889192>.
- 894 Al-Oqaili, F., Good, S.P., Peters, R.T., Finkenbiner, C., Sarwar, A. Using stable water isotopes to assess  
 895 the influence of irrigation structural configurations on evaporation losses in semiarid agricultural systems.  
 896 *Agricultural and Forest Meteorology*. 291: 108083, 2020.  
 897 <https://doi.org/10.1016/j.agrformet.2020.108083>.
- 898 Aragu, L., Froehlich, K., Rozanski, K. Stable isotope composition of precipitation over southeast Asia.  
 899 *Journal of Geophysical Research*. 103(28): 721-728, 1998. <https://doi.org/10.1029/98JD02582>.
- 900 Berg, A., Findell, K., Lintner, B., Giannini, A., Seneviratne, S.I., Hurk, B.V.D., Lorenz, R., Pitman, A.,  
 901 Hagemann, S., Meier, A. Land-atmosphere feedbacks amplify aridity increase over land under global  
 902 warming. *Nature Climate Change*. 6(9): 869-874, 2016. <https://doi.org/10.1038/nclimate3029>.
- 903 Beven, K., Germann, P. Macropores and water flow in soils revisited. *Water Resources Research*. 49(6):  
 904 3071-3092, 2013. <https://doi.org/10.1002/wrcr.20156>.
- 905 Bouwer, H. Artificial recharge of groundwater: hydrogeology and engineering. *Hydrogeology Journal*.  
 906 10(1): 121-142, 2002. <https://doi.org/10.1007/s10040-001-0182-4>.
- 907 Cai, H.E., Zhang, J.W., Zheng, J.G., Zhang, R.S., Liang, X.L. Hydrogeology features of Loess hilly gully  
 908 region in Yan'an. *Geotechnical Engineering Technique*. 33(5): 288-292, 2019.  
 909 <https://doi.org/10.3969/j.issn.1007-2993.2019.05.009>.
- 910 Chen, P.Y., Ma, J.Z., Ma, X.Y., Yu, Q., Cui, X.K., Guo, J.B. Groundwater recharge in typical geomorphic  
 911 landscapes and different land use types on the loess plateau, China. *Hydrological Processes*. 37(4): 14860,  
 912 2023. <https://doi.org/10.1002/hyp.14860>.
- 913 Dane, J.H., Topp, C.G., Gee, G.W. 2.4 Particle-Size Analysis. 5: 255-293, 2002.
- 914 Dasgupta, B., Prakash, P., Sen, R., Noble, J., Chatterjee, S., Sanyal, P. The isotopic composition of the  
 915 world' s highest river basins: Role of hydrological mixing ratios and transit time. *Journal of Hydrology*.  
 916 638: 131544, 2024. <https://doi.org/10.1016/j.jhydrol.2024.131544>.
- 917 Feng, X.M., Fu, B.J., Piao, S.L., Wang, S., Ciais, P., Zeng, Z.Z., Lü, Y.H., Zeng, Y., Li, Y., Jiang, X.H.,  
 918 Wu, B.F. Revegetation in China's Loess Plateau is approaching sustainable water resource limits. *Nature*  
 919 *Climate Change*. 6: 1019-1022, 2016. <https://doi.org/10.1038/nclimate3092>.





- 920 Fu, B.J., Chen, L., Ma, K. The effect of land use change on the regional environment in the Yangjuangou  
 921 catchment in the loess plateau of China. *Acta Geographica Sinica*. 54: 241-246, 1999.  
 922 <https://doi.org/10.3321/j.issn:0375-5444.1999.03.006>.
- 923 Fu, B.J., Liu, Y., Lü, Y.H., He, C.S., Zeng, Y., Wu, B.F. Assessing the soil erosion control service of  
 924 ecosystems change in the Loess Plateau of China. *Ecological Complexity*. 8 (4): 284-293, 2011.  
 925 <https://doi.org/10.1016/j.ecocom.2011.07.003>.
- 926 Fu, B.J., Wang, S., Liu, Y., Liu, J., Liang, W., Miao, C. Hydrogeomorphic ecosystem responses to natural  
 927 and anthropogenic changes in the Loess Plateau of China. *Annual Review of Earth and Planetary*  
 928 *Sciences*. 45: 223-243, 2017. <https://doi.org/10.1146/annurev-earth-063016-020552>.
- 929 Gates, J.B., Scanlon, B.R., Mu, X.M., Zhang, L. Impacts of soil conservation on groundwater recharge in  
 930 the semi-arid Loess Plateau, China. *Hydrogeology Journal*. 19(4): 865-875, 2011.  
 931 <https://doi.org/10.1007/s10040-011-0716-3>.
- 932 Gee, G. W., Hillel, D. Groundwater recharge in arid regions: Review and critique of estimation methods.  
 933 *Hydrological Processes*. 2(3): 255-266, 1988. <https://doi.org/10.1002/hyp.3360020306>.
- 934 Gleeson, T., Befus, K.M., Jasechko, S., Luijendijk, E., Cardenas, M.B. The global volume and  
 935 distribution of modern groundwater. *Nature Geoscience*. 9(2): 161-167, 2016. DOI: 10.1038/NGEO2590.
- 936 Gumuła-Kawęcka, A., Jaworska-Szulc B., Szymkiewicz A., Gorczewska-Langner W., Pruszkowska-  
 937 Caceres M., Angulo-Jaramillo R., Šimůnek J. Estimation of groundwater recharge in a shallow sandy  
 938 aquifer using unsaturated zone modeling and water table fluctuation method. *Journal of Hydrology*. 605:  
 939 127283, 2022. DOI: 10.1016/j.jhydrol.2021.127283.
- 940 He, M.N., Wang, Y.Q., Tong, Y.P., Zhao, Y.L., Qiang, X.K., Song, Y.G., Wang, L., Song, Y., Wang, G.D.,  
 941 He, C.X. Evaluation of the environmental effects of intensive land consolidation: A field-based case  
 942 study of the Chinese Loess Plateau. *Land Use Policy*. 94: 104523, 2020. DOI:  
 943 10.1016/j.landusepol.2020.104523.
- 944 Healy, R.W., Cook, P.G. Using groundwater levels to estimate recharge. *Hydrogeology Journal*. 10(1):  
 945 91-109, 2002. DOI: 10.1007/s10040-001-0178-0.
- 946 Heppner, C.S., Nimmo, J.R. A computer program for predicting recharge with a master recession curve.  
 947 U.S. Geological Survey Scientific Investigations Report. 2005-5172, 2005.  
 948 <https://doi.org/10.3133/sir20055172>.
- 949 Huang, J., Li, Y., Fu, C., Chen, F., Fu, Q., Dai, A., Wang, G. Dryland climate change: Recent progress



950 and challenges. *Reviews of Geophysics*. 55(3): 719-778, 2017. DOI: 10.1002/2016RG000550.

951 Huang, T.M., Pang, Z.H. Estimating groundwater recharge following land-use change using chloride  
 952 mass balance of soil profiles: a case study at Guyuan and Xifeng in the Loess Plateau of China.  
 953 *Hydrogeology Journal*. 19: 177-186, 2011. DOI: 10.1007/s10040-010-0643-8.

954 Huang, T.M., Pang, Z.H., Edmunds, W.M. Soil profile evolution following land-use change: Implications  
 955 for groundwater quantity and quality. *Hydrological Processes*. 27(8): 1238-1252, 2013. DOI:  
 956 10.1002/hyp.9302.

957 Huang, Y.N., Evaristo, J., Li, Z. Multiple tracers reveal different groundwater recharge mechanisms in  
 958 deep loess deposits. *Geoderma*. 353: 207-212, 2019. DOI: 10.1016/j.geoderma.2019.06.041.

959 Jasechko, S., Perrone, D. Global groundwater wells at risk of running dry. *Science*. 372(6540): 418-421,  
 960 2021. DOI: 10.1126/science.abc2755.

961 Ji, M.Y., Jia, D.B., Hao, Y.S., Liu, T., Yang, L.N., Li X.Y., Lv, C.G., Shang Z.Q. Hydrochemical and  
 962 isotopic characteristics and water transformation relationships in the Zhenglan Banner section of  
 963 Shandian River Basin. *Chinese Journal of Applied Ecology*. 1-11, 2024. DOI: 10.13287/j.1001-  
 964 9332.202410.015.

965 Jia, X.X., Zhu, P., Wei, X.R., Zhu, Y.J., Huang, M.B., Hu, W., Wang, Y.Q., Turkeltaub, T., Binley, A.,  
 966 Horton, R., Shao, M.A. Bringing ancient loess critical zones into a new era of sustainable development  
 967 goals. *Earth-Science Reviews*. 255: 104852, 2024. <https://doi.org/10.1016/j.earscirev.2024.104852>.

968 Jin, Z., Guo, L., Wang, Y.Q., Yu, X.L., Lin, H., Chen, Y.P., Chu, G.C., Zhang, J., Zhang, N.P. Valley  
 969 reshaping and damming induce water table rise and soil salinization on the Chinese Loess Plateau.  
 970 *Geoderma*. 339: 115-125, 2019. <https://doi.org/10.1016/j.geoderma.2018.12.048>.

971 Kuang, X.X., Luo, X., Jiao, J.J., Liang, S.H., Zhang, X.L., Li, H.L., Liu, J.G. Using stable isotopes of  
 972 surface water and groundwater to quantify moisture sources across the Yellow River source region.  
 973 *Hydrological Processes*. 33(13): 1835-1850, 2019. DOI: 10.1002/hyp.13441.

974 Kumar, A., Sanyal, P., Agrawal, S. Spatial distribution of  $\delta^{18}\text{O}$  values in river water in the Ganga River  
 975 Basin: insight into the hydrological processes. *Journal of Hydrology*. 571: 225-234, 2019. DOI:  
 976 10.1016/j.jhydrol.2019.01.044.

977 Lai, J.S., Zou, Y., Zhang, J.L., Peres-Neto, P.R. Generalizing hierarchical and variation partitioning in  
 978 multiple regression and canonical analyses using the *rdacca.hp* R package. *Methods in Ecology and*  
 979 *Evolution*. 13(4): 782-788, 2022. DOI: 10.1111/2041-210X.13800.



- 980 Lamontagne, S., Kirby, J., Johnston, C. Groundwater-surface water connectivity in a chain of ponds  
981 semiarid river. *Hydrological Processes*. 35(4): e14129, 2021. DOI: 10.1002/hyp.14129.
- 982 Letz, O., Siebner, H., Avrahamov, N., Egozi, R., Eshel, G., Dahan, O. The impact of geomorphology on  
983 groundwater recharge in a semi-arid mountainous area. *Journal of Hydrology*. 603: 127029, 2021. DOI:  
984 10.1016/j.jhydrol.2021.127029.
- 985 Li, H., Xiang, W., Si, B.C., Min, M., Miao, C.H., Jin, J.J. Quantifying recharge mechanisms in low-hilly  
986 areas of a loess region: Implications for the quantity and quality of groundwater. *Journal of Hydrology*.  
987 643: 131982, 2024. DOI: 10.1016/j.jhydrol.2024.131982.
- 988 Li, H.X., Han, S.B., Wu, X., Wang, S., Liu, W.P., Ma, T., Zhang, M.N., Wei, Y.T., Yuan, F.Q., Yuan, L.,  
989 Li, F.C., Wu, B., Wang, Y.S., Zhao, M.M., Yang, H.W., Wei, S.B. Distribution, characteristics and  
990 influencing factors of fresh groundwater resources in the Loess Plateau, China. *China Geology*. 4(3):  
991 209-526, 2021. DOI: 10.31035/cg2021057.
- 992 Li, Y. S. Effects of forest on water circle on the Loess Plateau. *Journal of Natural Resources*. 16(05):  
993 427-432, 2001. DOI: 111451567011-81/4190641.
- 994 Li, Y.R., Shi, W.H., Aydin, A., Beroya-Eitner, M.A., Gao, G.H. Loess genesis and worldwide distribution.  
995 *Earth-Science Reviews*. 201: 102947, 2020. <https://doi.org/10.1016/j.earscirev.2019.102947>.
- 996 Li, Z., Chen, X., Liu, W.Z., Si, B.C. Determination of groundwater recharge mechanism in the deep  
997 loessial unsaturated zone by environmental tracers. *Science of The Total Environment*. 586: 827-835,  
998 2017. <https://doi.org/10.1016/j.scitotenv.2017.02.061>.
- 999 Li, Z., Coles, A.E., Xiao, J. Groundwater and streamflow sources in China's Loess Plateau on catchment  
1000 scale. *Catena*. 181: 104075, 2019. <https://doi.org/10.1016/j.catena.2019.104075>.
- 1001 Lian, H.S., Yen, H., Yu, K., Zou, J.Y., Liu, C.X. Groundwater pollution becomes new constraint after  
1002 watershed-scale water quality restoration. *Journal of Hydrology*. 661: 133558, 2025.  
1003 <https://doi.org/10.1016/j.jhydrol.2025.133558>.
- 1004 Liang, W., Bai, D., Wang, F.Y., Fu, B.J., Yan, J.P., Wang, S., Yang T.Y., Long, D., Feng, M.Q. Quantifying  
1005 the impacts of climate change and ecological restoration on streamflow changes based on a Budyko  
1006 hydrological model in China's Loess Plateau. *Water Resources Research*. 51: 6500-6519, 2015. DOI:  
1007 10.1002/2014WR016589.
- 1008 Liang, X.J. *Applied hydrogeology*. Beijing: Science Press, 2016.
- 1009 Liu, D.S. *Loess and the environment*. Science Press, Beijing, 1985.



- 1010 Liu, X., Song, X.F., Zhang, Y.H., Xia, J., Zhang, X.C., Yu, J.J., Long, D., Li, F.D., Zhang, B. Spatio-  
1011 temporal variations of  $\delta^2\text{H}$  and  $\delta^{18}\text{O}$  in precipitation and shallow groundwater in the Hilly Loess Region  
1012 of the Loess Plateau, China. *Environmental Earth Sciences*. 63(5): 1105 – 1118, 2011. DOI:  
1013 10.1007/s12665-010-0785-y.
- 1014 Liu, Y.S., Chen, Z., Li, Y., Feng, W., Cao, Z. The planting technology and industrial development  
1015 prospects of forage rape in the loess hilly area: A case study of newly-increased cultivated land through  
1016 gully land consolidation in Yan'an, Shaanxi Province. *Journal of Natural Resources*. 32: 2065-2074, 2017.  
1017 DOI: 10.11849/zrzyxb.20161142.
- 1018 Liu, Y.S., Li, Y. Engineering philosophy and design scheme of gully land consolidation in Loess Plateau.  
1019 *Transactions of the Chinese Society of Agricultural Engineering*. 33(10): 1-9, 2017.
- 1020 Lu, Y.W. Study on typical hydrological characteristics of the vadose zone and spatiotemporal evolution  
1021 of potential groundwater recharge in the Chinese Loess Plateau. Yangling: Northwest A & F University,  
1022 2020. DOI: 10.11975/j.issn.1002-6819.2017.10.001.
- 1023 Lupi, L., Bertrand, L., Monferrón, M. V., Amé, M. V., del Pilar Diaz, M. Multilevel and structural  
1024 equation modeling approach to identify spatiotemporal patterns and source characterization of metals  
1025 and metalloids in surface water and sediment of the Ctalamochita River in Pampa region, Argentina.  
1026 *Journal of Hydrology*. 572: 403-413, 2019. <https://doi.org/10.1016/j.jhydrol.2019.03.019>.
- 1027 Manna, F., Murray, S., Abbey, D., Martin, P., Cherry, J., Parker, B. Spatial and temporal variability of  
1028 groundwater recharge in a sandstone aquifer in a semi-arid region. *Hydrology and Earth System Sciences*  
1029 *Discussions*. 2018: 1-36, 2018. <https://doi.org/10.5194/hess-23-2187-2019>.
- 1030 Medici, G., Munn, J. D., Parker, B. L. Delineating aquitard characteristics within a Silurian dolostone  
1031 aquifer using high-density hydraulic head and fracture datasets. *Hydrogeology Journal*. 32(6): 1663-1691,  
1032 2024. <https://doi.org/10.1007/s10040-024-02824-9>.
- 1033 Meles, M.B., Bradford, S., Casillas-Trasvina, A., Chen, L., Osterman, G., Hatch, T., Ajami, H., Crompton,  
1034 O., Levers, L., Kisekka, I. Uncovering the gaps in managed aquifer recharge for sustainable groundwater  
1035 management: A focus on hillslopes and mountains. *Journal of Hydrology*. 639: 131615, 2024. DOI:  
1036 10.1016/j.jhydrol.2024.131615.
- 1037 Nachabe, M.H. Analytical expressions for transient specific yield and shallow water table drainage.  
1038 *Water Resources Research*. 38 (10): 11-17, 2022. DOI: 10.1029/2001WR001071.
- 1039 Nicholson, S. E. *Dryland Climatology*. Cambridge University Press, 2011.



- 1040 Obuobie, E., Diekkruieger, B., Agyekum, W., Agodzo, S. Groundwater level monitoring and recharge  
1041 estimation in the White Volta River basin of Ghana. *Journal of African Earth Sciences*. 71-72: 80-86,  
1042 2012. DOI: 10.1016/j.jafrearsci.2012.06.005.
- 1043 Ouali, A.E., Roubil, A., Lahrach, A., Hmaidi, A.E., Ouali, A.E., Ousmana, H., Bouchaou, L. Assessments  
1044 of groundwater recharge process and residence time using hydrochemical and isotopic tracers under arid  
1045 climate: Insights from Errachidia basin (Central-East Morocco). *Groundwater for Sustainable*  
1046 *Development*. 25: 101145, 2024. DOI: 10.1016/j.gsd.2024.101145.
- 1047 Owuor, S. O., Butterbach-Bahl, K., Guzha, A. C., Rufino, M. C., Pelster, D. E., Díaz-Pinés, E., Breuer,  
1048 L. Groundwater recharge rates and surface runoff response to land use and land cover changes in semi-  
1049 arid environments. *Ecological Processes*, 5: 1-21, 2016. DOI: 10.1186/s13717-016-0060-6.
- 1050 Pe'csi, M. Loess is not just the accumulation of dust. *Quat Int.* 7(8):1-21, 1990. DOI:10.1016/1040-  
1051 6182(90)90034-2.
- 1052 Qiao, J.B., Zhu, Y.J., Jia, X.X., Huang, L.M., Shao, M.A. Spatial variability of soil water for the entire  
1053 profile in the critical zone of the Loess Plateau. *Advances in Water Science*. 28(04): 515-522, 2017. DOI:  
1054 10.14042/j.cnki.32.1309.2017.04.005.
- 1055 Qu, S., Zhao, Y.Z., Li, M.H., Ren, X.H., Wang, C.Y., Yang, X., Hao, Y.L., Dong, S.G., Yu, R.H. Unveiling  
1056 sources and fate of sulfate in lake-groundwater system combined Bayesian isotope mixing model with  
1057 radon mass balance model. *Water Research*. 282: 123648, 2025. 10.1016/j.watres.2025.123648.
- 1058 Salek, M., Levison, J., Parker, B., Gharabaghi, B. CAD-DRASTIC: chloride application density  
1059 combined with DRASTIC for assessing groundwater vulnerability to road salt application. *Hydrogeology*  
1060 *Journal*. 26: 2379-2393, 2018. DOI: 10.1007/s10040-018-1801-7.
- 1061 Scanlon, B.R., Healy, R.W., Cook, P.G. Choosing appropriate techniques for quantifying groundwater  
1062 recharge. *Hydrogeology Journal*. 10(1): 18-39, 2022. DOI: 10.1007/s10040-001-0176-2.
- 1063 Shah, N., Ross, M. Variability in specific yield under shallow water table conditions. *Journal of*  
1064 *Hydrologic Engineering*. 14(12): 1290-1298, 2009. [https://doi.org/10.1061/\(ASCE\)HE.1943-](https://doi.org/10.1061/(ASCE)HE.1943-5584.0000121)  
1065 [5584.0000121](https://doi.org/10.1061/(ASCE)HE.1943-5584.0000121).
- 1066 Shi, H., Shao, M.A. Soil and water loss from the Loess Plateau in China. *Journal of arid environments*.  
1067 45(1): 9-20, 2020. <https://doi.org/10.1006/jare.1999.0618>.
- 1068 Shi, P.J., Huang, Y.N., Yang, K.Y., Li, Z. Quantitative estimation of groundwater recharge in the thick  
1069 loess deposits using multiple environmental tracers and methods. *Journal of Hydrology*. 603(8): 126895,



- 1070 2021. <https://doi.org/10.1016/j.jhydrol.2021.126895>.
- 1071 Tan, H.B., Liu, Z.H., Rao, W.B., Jin, B., Zhang, Y.D. Understanding recharge in soil-groundwater
- 1072 systems in high loess hills on the Loess Plateau using isotopic data. *Catena*. 156: 18-29, 2017.
- 1073 <https://doi.org/10.1016/j.catena.2017.03.022>.
- 1074 Tan, H.B., Wen, X.W., Rao, W.B., Bradd, J., Huang, J.Z. Temporal variation of stable isotopes in a
- 1075 precipitation-groundwater system: implications for determining the mechanism of groundwater recharge
- 1076 in high mountain hills of the Loess Plateau, China. *Hydrological Processes*. 30(10): 1491-1505, 2016.
- 1077 <https://doi.org/10.1002/hyp.10729>.
- 1078 Tetzlaff, D., Seibert, J., McGuire, K.J., Laudon, H., Burns, D.A., Dunn, S.M., Soulsby, C. How does
- 1079 landscape structure influence catchment transit time across different geomorphic provinces?
- 1080 *Hydrological Processes*. 23: 945-953, 2009. <https://doi.org/10.1002/hyp.7240>.
- 1081 Tooth, S. Arid geomorphology: Changing perspectives on timescales of change. *Progress in Physical*
- 1082 *Geography*. 36(2): 262-284, 2012. DOI: 10.1177/0309133311417943.
- 1083 Vries, J.J.D., Simmers, I. Groundwater recharge: an overview of processes and challenges. *Hydrogeology*
- 1084 *Journal*. 10(1): 5-17, 2002. DOI: 10.1007/s10040-001-0171-7.
- 1085 Wan, H., Liu, W.G. An isotope study ( $\delta^{18}\text{O}$  and  $\delta^2\text{H}$ ) of water movements on the Loess Plateau of China
- 1086 in arid and semiarid climates. *Ecological Engineering*. 8(93): 226-233, 2016.
- 1087 <https://doi.org/10.1016/j.ecoleng.2016.05.039>
- 1088 Wang, L., Shao, M., Wang, Q.J., Gale, J. Historical changes in the environment of the Chinese Loess
- 1089 Plateau. *Environmental Science & Policy*. 9: 675-684, 2006.
- 1090 <https://doi.org/10.1016/j.envsci.2006.08.003>.
- 1091 Wang, W.Z., Sun, J.N., Xia, Y., Li, Z. Identifying hydraulic connectivity among the vadose zone,
- 1092 unconfined and confined aquifers in the thick loess deposits using multiple tracers. *Journal of Hydrology*.
- 1093 626: 130339, 2023. <https://doi.org/10.1016/j.jhydrol.2023.130339>.
- 1094 Wang, W.Z., Xia, Y., Sun, J.N., Liu, Y.Z., Li, P.Y., Han, F.P., Li, Z. Uncertainties in physical and tracer
- 1095 methods in actual groundwater recharge estimation in the thick loess deposits of China. *Journal of*
- 1096 *Hydrology*. 634: 131127, 2024. <https://doi.org/10.1016/j.jhydrol.2024.131127>.
- 1097 Wang, Y.Q., Shao, M.A., Sun, H., Fu, Z.H., Fan, J., Hu, W., Fang, L.C. Response of deep soil drought to
- 1098 precipitation, land use and topography across a semiarid watershed. *Agricultural and Forest Meteorology*.
- 1099 282-283: 107866, 2020. <https://doi.org/10.1016/j.agrformet.2019.107866>.



- 1100 Wang, Y.Q., Sun, H., Zhao, Y.L. Characterizing spatial-temporal patterns and abrupt changes in deep soil
- 1101 moisture across an intensively managed watershed. *Geoderma*. 341: 181-194, 2019.
- 1102 <https://doi.org/10.1016/j.geoderma.2019.01.044>.
- 1103 Wu, M.L. The structural equation model: AMOS operation and application. Chongqing: Chongqing
- 1104 University Press, 2010.
- 1105 Xiang W. Study on soil evaporation and groundwater recharge based on stable isotopes in the Loess
- 1106 Plateau at regional scale. Yangling: Northwest A & F University, 2020. DOI:
- 1107 10.27409/d.cnki.gxbnu.2021.000025.
- 1108 Xie, T.T., Zhao, H.J., Chen, G.K., Lin, H.H. Land Use Patterns and River Nitrate Dynamics in Karst
- 1109 Regions: Insights from High-Resolution Sentinel-2 Imagery and Partial Least Squares Structural
- 1110 Equation Modeling Analysis. *Environmental Engineering Science*, 2025.
- 1111 <https://doi.org/10.1089/ees.2024.0272>.
- 1112 Xu, P., Weng, B.S., Gong, X.Y., Xia, K.B., Yan, D.H., Wang, H. Estimation of shallow groundwater
- 1113 recharge in central Qinghai-Tibet Plateau by combining unsaturated zone simulation and improved water
- 1114 table fluctuation method. *Journal of Hydrology*. 630: 130689, 2024.
- 1115 <https://doi.org/10.1016/j.jhydrol.2024.130689>.
- 1116 Xu, Y., Beekman, H. E. Review: Groundwater recharge estimation in arid and semi-arid southern Africa.
- 1117 *Hydrogeology Journal*. 27(3): 929-943, 2019. DOI: 10.1007/s10040-018-1898-8.
- 1118 Xu, Z.Y., Zhao, Y.J., Chen, J.J. Research of fractural efficacy on mechanisms governing water flow in
- 1119 unsaturated loess. *Journal of Changchun University of Earth Sciences*. 23(03): 326-329, 1993.
- 1120 Xue, S.B., Li, P., Cui, Z.W., Li, Z.B. The influence of different check dam configurations on the
- 1121 downstream river topography and water-sediment relationship. *Journal of Hydrology*. 656: 133046, 2025.
- 1122 DOI: 10.1016/j.jhydrol.2025.133046.
- 1123 Yan, T.B., Wang, D.Q. The Recharge Mechanism of Unconfined Groundwater in the Loess of the
- 1124 Luochuan Yuan and Its Water Bearing Characteristics. *Geological Review*. 5(29): 418-427, 1983.
- 1125 Yang, N., Wang, G.C. Spatial variation of water stable isotopes of multiple rivers in southeastern Qaidam
- 1126 Basin, northeast Qinghai-Tibetan Plateau: Insights into hydrologic cycle. *Journal of Hydrology*. 628:
- 1127 130464, 2023. <https://doi.org/10.1016/j.jhydrol.2023.130464>.
- 1128 Yang, X.P., Liu, T., Yuan, B.Y. The Loess Plateau of China: Aeolian sedimentation and fluvial erosion,
- 1129 both with superlative rates. *Geomorphological Landscapes of the World*. 1: 275-282, 2009. DOI:



- 1130 10.1007/978-90-481-3055-9\_28.
- 1131 Yu L.L., Ji, Z.X., Wang, L. Characteristics of Perched Water Recharge in the Dam Land of Yangjuangou
- 1132 Small Watershed on the Loess Plateau. *Acta Pedologica Sinica*. 62(4): 983-997, 2025. DOI :
- 1133 10.11766/trxb202404290178.
- 1134 Yuan, S., Li, Z., Chen, L., Li, P., Zhang, Z., Zhang, J., Wang, A. Effects of a check dam system on the
- 1135 runoff generation and concentration processes of a catchment on the Loess Plateau. *International Soil*
- 1136 *and Water Conservation Research*. 10(1): 86-98, 2022. <https://doi.org/10.1016/j.iswcr.2021.06.007>.
- 1137 Zhang, H., Xu, Y.X., Kanyerere, T. A review of the managed aquifer recharge: Historical development,
- 1138 current situation and perspectives. *Physics and Chemistry of the Earth, Parts A/B/C*. 118-119: 102887,
- 1139 2020. DOI: 10.1016/j.pce.2020.102887.
- 1140 Zhang, J., Chen, H.S., Fu, Z.Y., Wang, F., Wang, K.L. Towards hydrological connectivity in the karst
- 1141 hillslope critical zone: Insight from using water isotope signals. *Journal of Hydrology*. 617: 128926, 2022.
- 1142 DOI: 10.1016/j.jhydrol.2022.128926.
- 1143 Zhang, Y.H., Wu, Y.P. Oxygen and Hydrogen Isotopes in Precipitation in Heihe River Basin, China.
- 1144 *Journal of Glaciology and Geocryology*. 31(1): 34-39, 2009. DOI: 100020240(2009)0120034206.
- 1145 Zhao, Y. L., Wang, Y.Q., Sun, H., Lin, H., Jin, Z., He, M.N., Yu, Y. L., Zhou, W. J., and An, Z. S. Intensive
- 1146 land restoration profoundly alters the spatial and seasonal patterns of deep soil water storage at watershed
- 1147 scales. *Agriculture, Ecosystems & Environment*. 280: 129-141, 2019.
- 1148 <https://doi.org/10.1016/j.agee.2019.04.028>.
- 1149 Zhao, Y., Wang, L. Determination of groundwater recharge processes and evaluation of the ‘two water
- 1150 worlds’ hypothesis at a check dam on the Loess Plateau. *Journal of Hydrology*. 595: 125989, 2021.
- 1151 <https://doi.org/10.1016/j.jhydrol.2021.125989>.
- 1152 Zhao, Y.L., Wang, Y.Q., Hu, W., Sun, H., Qi, L.J., Xu, L., Song, Y., Zhang, P.P. Intensive land restoration
- 1153 projects alter mechanisms underpinning spatiotemporal soil moisture variability at a catchment scale: A
- 1154 case study in China. *Journal of Hydrology*. 630: 130739, 2024.
- 1155 <https://doi.org/10.1016/j.jhydrol.2024.130739>.
- 1156 Zhao, Y.L., Wang, Y.Q., Zhou, J.X., Qi, L.J., Zhang, P.P. Spatiotemporal variation and controlling factors
- 1157 of dried soil layers in a semi-humid catchment and relevant land use management implications. *CATENA*.
- 1158 240: 107973, 2024. <https://doi.org/10.1016/j.catena.2024.107973>.
- 1159 Zhu, Y.J., Jia, X.X., Shao, M.A. Loess thickness variations across the loess plateau of China. *Surveys in*



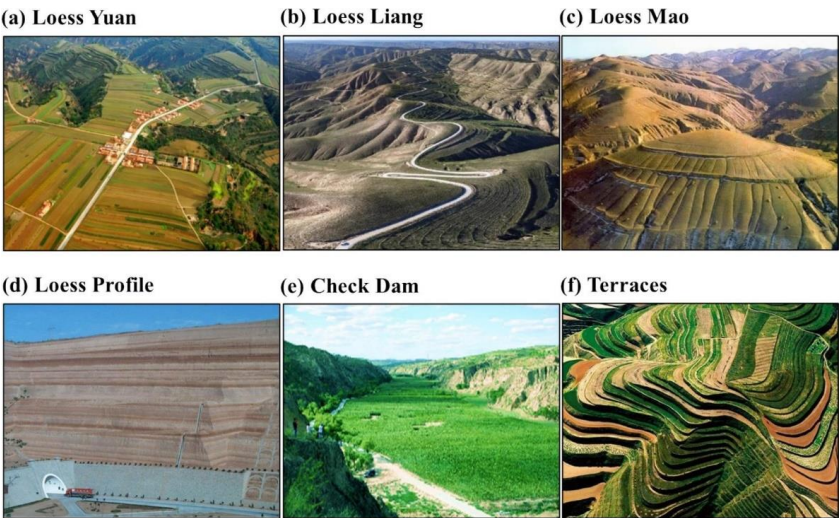


1160 Geophysics. 39(4): 715-727, 2018. <https://doi.org/10.1007/s10712-018-9462-6>.



1161 **Appendix A**

1162 1. The typical loess landforms on the Loess Plateau is shown.



1163  
1164 Fig. A1. Typical loess landforms are (a) Loess Yuan, (b) Loess Liang, and (c) Loess Mao. (d) A loess  
1165 profile, (e) check dams and (f) terraces on the Chinese Loess Plateau. (adapted from Jia et al., 2024)

1166 2. The specific yield of different soil textures is shown.

1167 Table A1. The specific yield of different texture of soil (adapted from Liang, 2016)

Texture	Average Specific	Minimum	Maximum Specific	Coefficient of
	Yield	Specific Yield	Yield	Variation (%)
Clay	0.02	0.00	0.05	59
Silt	0.08	0.03	0.19	60
Sandy Clay	0.07	0.03	0.12	44
Fine Sand	0.21	0.10	0.28	32
Medium Sand	0.26	0.15	0.32	18
Coarse Sand	0.27	0.20	0.35	18
Gravelly Sand	0.25	0.20	0.35	21
Fine Gravel	0.25	0.21	0.35	18
Medium Gravel	0.23	0.13	0.26	14
Coarse Gravel	0.22	0.12	0.26	20

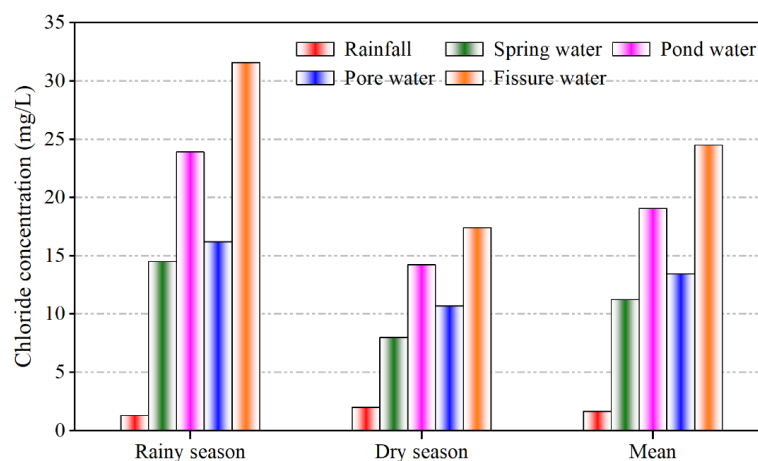


1168 3. The isotopic composition ( $\delta^2\text{H}$  and  $\delta^{18}\text{O}$ ) of various water sources in the rainy and dry seasons is shown.

1169 Table A2. Isotopic composition ( $\delta^2\text{H}$  and  $\delta^{18}\text{O}$ ) of various water sources in the rainy and dry seasons

	Rainy season		Dry season	
	$\delta^2\text{H}$	$\delta^{18}\text{O}$	$\delta^2\text{H}$	$\delta^{18}\text{O}$
Rainfall	$-36.6 \pm 20.4\text{‰}$	$-5.6 \pm 2.3\text{‰}$	$-31.0 \pm 23.2\text{‰}$	$-4.9 \pm 3.0\text{‰}$
Pond water	$-40.5 \pm 13.1\text{‰}$	$-4.1 \pm 2.3\text{‰}$	$-24.5 \pm 6.9\text{‰}$	$-0.8 \pm 1.3\text{‰}$
Spring water	$-67.3 \pm 2.6\text{‰}$	$-9.0 \pm 0.4\text{‰}$	$-68.4 \pm 2.2\text{‰}$	$-9.0 \pm 0.4\text{‰}$
Pore water	$-66.3 \pm 3.1\text{‰}$	$-9.0 \pm 0.6\text{‰}$	$-65.4 \pm 3.8\text{‰}$	$-8.5 \pm 0.6\text{‰}$
Fissure water	$-65.0 \pm 3.8\text{‰}$	$-8.8 \pm 0.9\text{‰}$	$-64.5 \pm 5.5\text{‰}$	$-8.5 \pm 0.9\text{‰}$

1170 4. The chloride concentrations of various water sources in the rainy and dry seasons is shown.



1171

1172 Fig. A2. Chloride concentrations of various water sources in the rainy and dry seasons.